Available online at www.sciencedirect.com
ScienceDirect
Journal of Computational and Applied Mathematics 209 (2007) 246–266
JOURNAL OF COMPUTATIONAL AND APPLIED MATHEMATICS
www.elsevier.com/locate/cam

Evaluating the boundary and covering degree of planar Minkowski sums and other geometrical convolutions

Rida T. Farouki[a,*], Joel Hass[b]

[a] *Department of Mechanical and Aeronautical Engineering, University of California, Davis, CA 95616, USA*
[b] *Department of Mathematics, University of California, Davis, CA 95616, USA*

Received 5 February 2006; received in revised form 4 August 2006

Abstract

Algorithms are developed, based on topological principles, to evaluate the boundary and "internal structure" of the Minkowski sum of two planar curves. A graph isotopic to the envelope curve is constructed by computing its *characteristic points*. The edges of this graph are in one-to-one correspondence with a set of monotone envelope segments. A simple formula allows a *degree* to be assigned to each face defined by the graph, indicating the number of times its points are covered by the Minkowski sum. The boundary can then be identified with the set of edges that separate faces of zero and non-zero degree, and the boundary segments corresponding to these edges can be approximated to any desired geometrical accuracy. For applications that require only the Minkowski sum boundary, the algorithm minimizes geometrical computations on the "internal" envelope edges, that do not contribute to the final boundary. In other applications, this internal structure is of interest, and the algorithm provides comprehensive information on the covering degree for different regions within the Minkowski sum. Extensions of the algorithm to the computation of Minkowski sums in $\mathbb{R}^3$, and other forms of *geometrical convolution*, are briefly discussed.

MSC: 65D17; 65D18; 68U05; 68U07

Keywords: Minkowski sums; Geometrical convolutions; Covering degree; Planar graph; Topological configuration; Singular points; Gauss map; Curvature

1. Introduction and motivation

Interest in algorithms to compute Minkowski sums of point sets in $\mathbb{R}^2$ or $\mathbb{R}^3$ has grown rapidly in recent years, motivated by applications in computer-aided geometric design, computer graphics and animation, image processing, and path planning for manufacturing or inspection. Most current algorithms are concerned with sets that have polygonal boundaries. In this context the dominant issues are combinatorial in nature, and the algorithms are typically amenable to a rigorous asymptotic complexity analysis.

The emphasis in this paper is on efficient algorithms for Minkowski sums of sets in $\mathbb{R}^2$ with smooth curved boundaries. As a governing paradigm, these algorithms employ topological concepts to minimize intermediate calculations that do not contribute to the final Minkowski sum boundary. Identifying a set of *characteristic points* on the "envelope"

* Corresponding author.
E-mail addresses: farouki@ucdavis.edu (R.T. Farouki), hass@math.ucdavis.edu (J. Hass).

0377-0427/$ - see front matter © 2006 Published by Elsevier B.V.
doi:10.1016/j.cam.2006.11.006

curve, that constitutes a superset of the Minkowski sum boundary, allows a planar graph isotopic to this envelope to be constructed. Furthermore, each face of this graph is assigned a *degree* specifying the number of different ways it arises as a sum of points on the operand set boundaries. Graph edges corresponding to true Minkowski sum boundary segments can be readily identified as those that separate adjacent faces with zero and non-zero degree, and these boundary segments can then be approximated to any prescribed geometrical tolerance.

Minkowski sums are employed in this paper as an illustrative context for a broader family of point-set operations, that we call *geometrical convolutions*. The Minkowski sum $\mathscr{A} \oplus \mathscr{B}$ of point sets $\mathscr{A}, \mathscr{B} \in \mathbb{R}^n$ is defined [46,70] by

$$\mathscr{A} \oplus \mathscr{B} = \{\mathbf{a} + \mathbf{b} \,|\, \mathbf{a} \in \mathscr{A} \text{ and } \mathbf{b} \in \mathscr{B}\}, \tag{1}$$

and this can also be interpreted as

$$\mathscr{A} \oplus \mathscr{B} = \bigcup_{\mathbf{b} \in \mathscr{B}} (\mathscr{A} + \mathbf{b}), \tag{2}$$

where $\mathscr{A} + \mathbf{b}$ is the translate[1] of set $\mathscr{A}$ by point $\mathbf{b}$. Replacing set translations by more general geometrical transformations, a geometrical convolution $\mathscr{A} * \mathscr{B}$ of two point sets $\mathscr{A}, \mathscr{B} \in \mathbb{R}^n$ is defined as the union of a continuous family of transformations of set $\mathscr{A}$, corresponding to each point of set $\mathscr{B}$ (or vice versa)—namely,

$$\mathscr{A} * \mathscr{B} = \bigcup_{\mathbf{b} \in \mathscr{B}} T_{\mathbf{b}}(\mathscr{A}), \tag{3}$$

where $T_{\mathbf{b}}(\mathscr{A})$ denotes a given transformation[2] of set $\mathscr{A}$, smoothly dependent on position $\mathbf{b}$ in set $\mathscr{B}$. The mappings $T_{\mathbf{b}}$ defined on set $\mathscr{B}$ may be isometries (i.e., shape-preserving transformations) or, more generally, homeomorphisms (continuous one-to-one mappings that admit changes of shape). The point sets $\mathscr{A}$, $\mathscr{B}$ and $\mathscr{A} * \mathscr{B}$ typically reside in $\mathbb{R}^2$ or $\mathbb{R}^3$, but there are no essential restrictions on their individual set dimensions—they may be points, curves, surfaces, solids, or any combinations thereof.

Whereas *functional* convolutions are well-studied analytic tools in diverse scientific and engineering applications—e.g., the use of Fourier and Laplace transform methods in signal processing, design of imaging systems, and the dynamic characterization of control systems [16,22]—a unified theoretical and algorithmic framework for computing *geometrical* convolutions remains to be developed. The Minkowski sum problem is a natural point of departure towards this goal. In subsequent studies, the algorithms will be generalized to encompass a broader family of geometrical convolutions.

Specific types of geometrical convolution are employed in computer-aided geometric design [10,12,25,47,61,67,68,75]; image processing [43,79,80]; computer graphics and animation [3,23,56,72]; path planning for robots or mechanisms [19,42,57,63–65,86]; simulation of material removal in NC machining [52,53,66,78,84,85]; wavefront propagation in geometric optics [28,29]; and "interval arithmetic" for complex-number sets [27,37,38,73]. However, existing algorithms used in these applications are typically context-specific and rather inefficient. A unified theory of geometrical convolutions, based on fundamental topological and geometrical principles arising from definition (3) of $\mathscr{A} * \mathscr{B}$, is still lacking.

In computing the Minkowski sum boundary $\partial(\mathscr{A} \oplus \mathscr{B})$ or other convolution boundary $\partial(\mathscr{A} * \mathscr{B})$ of two regions $\mathscr{A}, \mathscr{B} \in \mathbb{R}^2$, we note that only points on the boundaries $\partial\mathscr{A}$, $\partial\mathscr{B}$ of the given sets contribute[3]—interior points of $\mathscr{A}$, $\mathscr{B}$ always generate interior points of the Minkowski sum or other convolution set. The algorithm proposed here differs from existing Minkowski sum algorithms [34,55,60] by invoking topological principles to defer detailed geometrical calculations as far as possible, a strategy that allows certain "unnecessary" computations to be bypassed. It is guaranteed to yield a topologically correct result, provided that the stated assumptions are met. This is not the case for algorithms based on piecewise-linear approximations of smooth curves, which can produce topologically incorrect results if the approximation is not sufficiently accurate—see Remark 1 in Section 3.

The algorithm computes a set of characteristic points on the Minkowski sum *envelope curve*—a superset of the true boundary—and these points are then used to construct a piecewise-linear graph, isotopic to the envelope. An elementary calculation at a representative point of each graph edge suffices to indicate how the covering degree changes upon

[1] Alternately, $\mathscr{A} \oplus \mathscr{B}$ can be viewed as a union of translates of set $\mathscr{B}$ by the points of $\mathscr{A}$.

[2] A precise definition requires careful attention to the nature of the transformation $T_{\mathbf{b}}$ and its dependence on $\mathbf{b}$, and will be discussed elsewhere.

[3] This is true whenever the transformations $T_{\mathbf{b}}$ for $\mathbf{b} \in \mathscr{B}$ in (3) are homeomorphisms.

crossing that edge. In this manner, the true boundary edges are identified without the need for extensive geometrical computations, and complete information on the variation of the covering degree is available for applications that require it.

The plan for this paper is as follows. After briefly surveying the concept of a geometrical convolution (and existing geometrical procedures it subsumes) in Section 2, the specific case of Minkowski sums of planar curves is addressed in Section 3. Analysis of the behavior of a Minkowski sum in the neighborhood of a sum of two points $\mathbf{a} \in \partial\mathscr{A}$, $\mathbf{b} \in \partial\mathscr{B}$ in Section 4 reveals how the covering of $\mathscr{A} \oplus \mathscr{B}$ changes as we cross an envelope segment. The identification of the *characteristic points* of the Minkowski sum envelope is discussed in Section 5—these points are used to construct a planar graph, isotopic to the envelope, by the curve description algorithm summarized in Section 6. The Minkowski sum algorithm, enumerated in Section 7, involves construction of this graph, assignment of a covering degree to each face delineated by it, identification of true boundary edges separating faces of zero and non-zero degree, and the approximation of these edges to a specified geometrical tolerance. Some important points in the generalization of this algorithm to other geometrical convolutions are briefly discussed in Section 8. Finally, the main results of the paper are recapitulated in Section 9, and directions for further research are suggested.

2. Geometrical convolutions

Although they constitute a natural counterpart to function convolutions, and subsume many known special-case geometrical constructions, the notion of *geometrical convolutions* has only been invoked in specific contexts—e.g., [24,51]. A systematic development of this concept, based on new algorithmic paradigms, seems overdue. The utility of expression (3) lies in its ability to accommodate a variety of input geometries and transformation types, while remaining amenable to analysis by fundamental topological and geometrical principles. A brief survey of the useful operations encompassed by expression (3) is presented here, and in Section 8 we address some key points that arise in extending the Minkowski sum algorithm (the main focus of this paper) to the broader context defined by (3).

2.1. Envelopes of curve families

In computing geometrical convolutions in $\mathbb{R}^2$, the concept of the *envelope* of a one-parameter family of curves $\mathscr{C}(\lambda)$ for $\lambda \in [0, 1]$ plays a key role. Given two curves, such a family is typically generated by applying a differentiable sequence of transformations, parameterized by the points of one of the curves, to the other curve. There are several essentially equivalent definitions for the envelope Γ of the curve family $\mathscr{C}(\lambda)$, which may be formulated as follows:

- The envelope Γ is the locus of the intersections of "neighboring" curves, $\mathscr{C}(\lambda)$ and $\mathscr{C}(\lambda + \Delta\lambda)$, in the limit $\Delta\lambda \to 0$.
- The envelope Γ is a curve that is tangent at some point to each member of the curve family $\mathscr{C}(\lambda)$.
- If $\mathscr{S}$ is the surface defined by "stacking" each curve $\mathscr{C}(\lambda)$ at height $z = \lambda$ above the (x, y) plane, the envelope Γ is the "critical set" (or *silhouette*) of the projection of $\mathscr{S}$ onto the (x, y) plane.

See [14,17,18,41] for complete details on these formulations. For a family of implicit curves $f(x, y, \lambda) = 0$, satisfaction of the equations

$$f(x, y, \lambda) = \frac{\partial f}{\partial \lambda}(x, y, \lambda) = 0$$

is a necessary condition for points on each curve λ of the family to lie on the envelope Γ. On the other hand, for a family of parametric curves $\mathbf{r}(t, \lambda)$ the necessary condition is expressed by parallelism of the partial derivatives,

$$\frac{\partial \mathbf{r}}{\partial t}(t, \lambda) \parallel \frac{\partial \mathbf{r}}{\partial \lambda}(t, \lambda).$$

We are primarily concerned here with the case where the members of the family $\mathscr{C}(\lambda)$ are smooth closed curves, and the domain $\lambda \in [0, 1]$ amounts to a parameterization of the unit circle S^1, so that $\mathscr{C}(1) = \mathscr{C}(0)$ and $\mathscr{C}'(1) = \mathscr{C}'(0)$. For a geometrical convolution that generates the family $\mathscr{C}(\lambda)$, the significance of the envelope Γ in this context is that it defines a *superset* of the boundary of the convolution region (Γ typically includes segments in the interior of

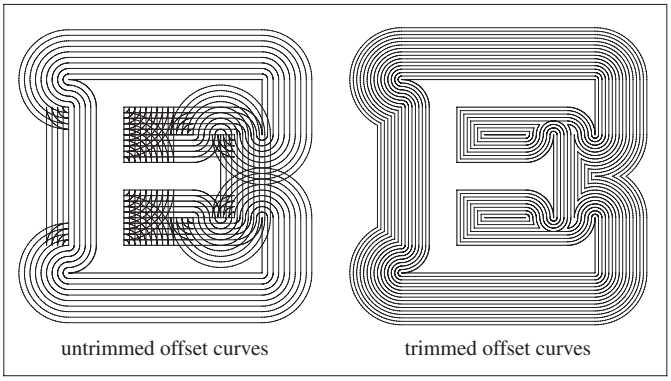

Fig. 1. A family of untrimmed and trimmed offsets to a piecewise-linear/circular curve. In this case, the offsets are likewise piecewise-linear/circular.

the convolution). In the case of a non-periodic curve family, with $\mathscr{C}(1) \neq \mathscr{C}(0)$, the envelope alone does not suffice to define the convolution boundary—portions of the initial and final curves $\mathscr{C}(0)$ and $\mathscr{C}(1)$ may also contribute to it. Hence, in this context, we define the *augmented envelope* by

$$\Gamma' = \mathscr{C}(0) \cup \Gamma \cup \mathscr{C}(1), \tag{4}$$

as a superset of the convolution boundary.

The envelope Γ is a superset of the convolution set boundary, since it is characterized by a necessary, but not sufficient, "local" condition for lying on the boundary (see below). Also, in the case of the augmented envelope (4), portions of the initial and final curves $\mathscr{C}(0)$, $\mathscr{C}(1)$ may lie in the interior of the convolution set, while others are on the boundary. The challenge is to develop an algorithm that identifies the true boundary, while minimizing "wasted" computations on portions of Γ that do not contribute to this boundary.

We now briefly survey a number of different operations that fall within the broad scope of *geometrical convolutions*. In Section 8 we outline how the algorithms developed here, for the specific case of Minkowski sums, can be extended to accommodate these other types of geometrical convolutions.

2.2. Offset curves and surfaces

For the Minkowski sum of a piecewise-smooth planar curve $\mathbf{r}(t)$ with unit normal $\mathbf{n}(t)$ and a circle of radius d, the envelope is the "untrimmed" *offset* (or *parallel*) curve

$$\mathbf{r}_d(t) = \mathbf{r}(t) \pm d\mathbf{n}(t). \tag{5}$$

At tangent discontinuities, $\mathbf{n}(t)$ is considered to rotate between its left and right limits. The *trimmed* (true) offset is typically obtained from (5) by use of a "trimming procedure" that employs global distance tests. Fig. 1 shows a sequence of untrimmed and trimmed (exterior) offsets to an "E" character.

Offset surfaces can be defined in an analogous manner [25], as envelopes of families of spheres of radius d whose centers lie on a given surface $\mathbf{r}(u, v)$. Offset curves and surfaces are used to define tool paths and tolerance zones in CAD/CAM [75] and related fields. Unfortunately, the offset to a rational curve of degree n is not,[4] in general, rational: it is (a subset of) an irreducible algebraic curve of degree $4n - 6$ [39]. This fact has spawned a profusion of approximation schemes for offsets—see, for example [23].

2.3. Minkowski products, powers, and roots

Minkowski sums have attracted interest as "shape operators" in $\mathbb{R}^2$ and $\mathbb{R}^3$ for use in computer graphics, animation, image processing, and computer-aided design [43,47,54–56,60,68,79,80]. The usual approach to computing Minkowski

[4] The Pythagorean–hodograph curves [26] are noteworthy exceptions: they incorporate special algebraic structures, ensuring rationality of their offset curves.

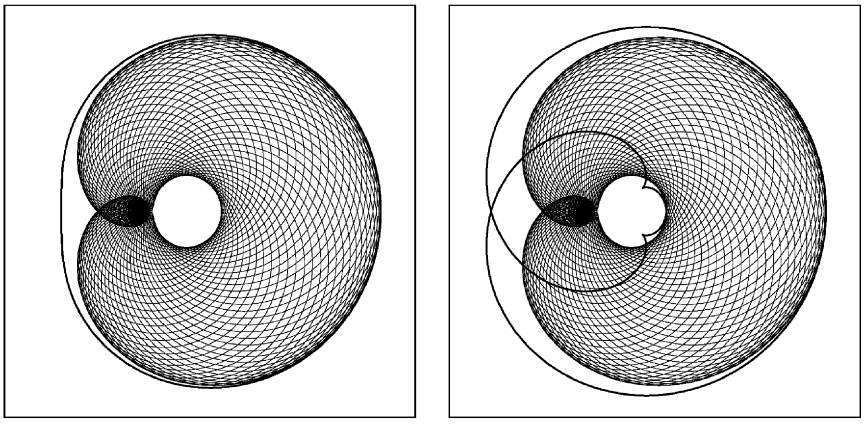

Fig. 2. The implicitly-defined set (7) when $\mathscr{A}$ and $\mathscr{B}$ are the circular disks $|\mathbf{z}| \leqslant 1$ and $|\mathbf{z}-1| \leqslant 1$, and $\mathbf{f}(\mathbf{a}, \mathbf{b}) = \mathbf{ab} + \mathbf{b}^2$. By the sub-distributive law of the Minkowski algebra, this set can be bounded by the combinations $(\mathscr{A} \oplus \mathscr{B}) \otimes \mathscr{B}$ as shown on the left, and $(\mathscr{A} \otimes \mathscr{B}) \oplus (\mathscr{B} \otimes \mathscr{B})$, on the right.

sums of point sets in $\mathbb{R}^2$ and $\mathbb{R}^3$ is to invoke the *Gauss maps* of their boundaries to determine appropriate segmentations. Sums of matched points (with parallel/anti-parallel normals) on corresponding segments then generate potential boundary segments of the Minkowski sum.

Definition (1) of the Minkowski sum of point sets $\mathscr{A}, \mathscr{B} \in \mathbb{R}^n$ can be adapted, in the case $n=2$, to define a Minkowski product

$$\mathscr{A} \otimes \mathscr{B} = \{\mathbf{a} \times \mathbf{b} \,|\, \mathbf{a} \in \mathscr{A} \text{ and } \mathbf{b} \in \mathscr{B}\}, \tag{6}$$

by interpreting $\times$ as complex multiplication. This offers a versatile algebra of point sets in $\mathbb{R}^2$ [37,38]. Apart from its interpretation as the extension of real interval arithmetic [71] to complex sets, this *Minkowski geometric algebra* has diverse applications in science and engineering, such as direct and inverse wavefront propagation in geometric optics [28,29,37], the stability analysis of dynamic systems with uncertain parameters [33,36], and as a framework for unifying and extending basic 2D shape operators.

Based on the Minkowski sum and product definitions, the algebra may be extended to encompass roots and powers of sets [30,40]; Minkowski values of polynomials over a given set [31]; and solutions of elementary equations for unknown sets [32]. Substituting a bivariate function (typically a polynomial) $\mathbf{f}(\mathbf{a}, \mathbf{b})$ for the sum $\mathbf{a}+\mathbf{b}$ or product $\mathbf{a} \times \mathbf{b}$ in (1) or (6), one may also consider *implicitly-defined sets* (see Fig. 2) of the form

$$\mathscr{A} \,\textcircled{\mathrm{f}}\, \mathscr{B} = \{\mathbf{f}(\mathbf{a}, \mathbf{b}) \,|\, \mathbf{a} \in \mathscr{A} \text{ and } \mathbf{b} \in \mathscr{B}\}. \tag{7}$$

Whereas Minkowski sums and products can be viewed as unions of translated and scaled/rotated copies of one set, expression (7) is even more versatile—for appropriately well-behaved functions $\mathbf{f}$, it can be interpreted as the union of a family of *conformal mappings* of one set.

2.4. Shape recovery from medial axis transform

The *medial axis* of a region in $\mathbb{R}^2$ is the locus of centers of inscribed disks, that touch the boundary in at least at two points. Similarly, the medial axis of a volume in $\mathbb{R}^3$ is the set of centers of inscribed spheres, that touch the boundary in at least three points. The *medial axis transform* (or MAT) comprises the medial axis with a superposed radius function, specifying the size of the inscribed disks or spheres. MATs facilitate the encoding, analysis, and comparison of shapes for applications in the life sciences, engineering, graphic design, and other contexts [13,15].

The computation of MATs for prescribed shapes has received considerable attention: see, for example [74] and references therein. The converse problem of *reconstruction* of a shape from its MAT can be considered a generalization of the offset curve problem, in which we desire the envelope of a family of *variable-radius* disks or spheres with a given locus of centers.

2.5. Swept surfaces and volumes

A *swept surface* is created by using a "sweep curve" to define the continuous action of a family of transformations on a "profile curve"—the union of the transformed instances of the profile curve constitutes the swept surface. The transformations may involve combinations of scaling, translation, rotation, affine mappings, etc., and the surface representation can be constructed by an elegant matrix algebra [35]. A *swept volume* is defined as the union of the instances of a rigid object that executes a general spatial motion (translation and rotation). Swept volumes are of fundamental importance in applications such as simulation of material removal from a stock workpiece by a five-axis CNC machine tool [52,53,66,84,85] and collision detection or avoidance in robot path planning [19,42,64,65]. Swept volumes in $\mathbb{R}^3$ are perhaps the most challenging convolutions from a computational perspective.

The computation of swept volumes has been addressed by many authors [1,3,9–12,57–59,61–63,67,72,78,83,84,86,87]. Most of these studies employ an envelope or differential-equation characterization for the swept-volume boundary. However, such conditions are only *sufficient* for belonging to the swept-volume boundary, and can generate topologically intricate structures exhibiting voids, self-intersections, and "internal faces". Such configurations can be difficult to compute, in part due to the inherent complexity of the singularities of surfaces in $\mathbb{R}^3$. An alternate approach, that minimizes computations on portions of the envelope that do not contribute to the swept-volume boundary, is therefore desirable.

3. Minkowski sums of plane curves

Let $\boldsymbol{\alpha}(u), u \in [0, 1]$ and $\boldsymbol{\beta}(v), v \in [0, 1]$ be smooth regularly parameterized[5] curves in $\mathbb{R}^2$, not necessarily embedded or closed (i.e., self-intersecting curves and curves with $\boldsymbol{\alpha}(1) \neq \boldsymbol{\alpha}(0)$ are allowed). We are interested in computing the Minkowski sum of $\boldsymbol{\alpha}(u)$, $\boldsymbol{\beta}(v)$. The solution of this problem is important for a much broader range of Minkowski sum computations in the plane. For example, the Minkowski sum of closed bounded sets $\mathscr{A}, \mathscr{B} \in \mathbb{R}^2$ can be found by computing the Minkowski sum of just the boundary curves $\partial\mathscr{A}$, $\partial\mathscr{B}$.

For sets with smooth boundaries $\partial\mathscr{A}$ and $\partial\mathscr{B}$, algorithms to compute the Minkowski sum boundary $\partial(\mathscr{A} \oplus \mathscr{B})$ typically invoke the fact that, in order for the sum $\mathbf{a} + \mathbf{b}$ of points $\mathbf{a} \in \partial\mathscr{A}$, $\mathbf{b} \in \partial\mathscr{B}$ to lie on $\partial(\mathscr{A} \oplus \mathscr{B})$, the boundary tangents or normals at those points must be either parallel or anti-parallel [54,55,60,61]—namely,

$$\partial(\mathscr{A} \oplus \mathscr{B}) \subseteq \{\mathbf{a} + \mathbf{b} \,|\, \mathbf{a} \in \partial\mathscr{A}, \mathbf{b} \in \partial\mathscr{B} \text{ and } \mathbf{t_a} = \pm\mathbf{t_b}\}, \tag{8}$$

where $\mathbf{t_a}$ and $\mathbf{t_b}$ are the tangents to the respective set boundaries at the points $\mathbf{a}$ and $\mathbf{b}$. Now the fact that the "matching" or *Jacobian* criterion $\mathbf{t_a} = \pm\mathbf{t_b}$ is just a necessary (not sufficient-and-necessary) condition for pairs of points from $\partial\mathscr{A}$, $\partial\mathscr{B}$ to generate points on $\partial(\mathscr{A} \oplus \mathscr{B})$ means that using this condition to simultaneously trace $\partial\mathscr{A}$, $\partial\mathscr{B}$ and adding the matched point pairs yields the *superset* of $\partial(\mathscr{A} \oplus \mathscr{B})$ defined by the right-hand side of (8)—called the *envelope*. To identify the true Minkowski sum boundary, a membership test must be performed on each region of the superset delineated by the envelope, and the appropriate boundary segments of the regions that pass must finally be organized into a data structure to faithfully describe $\partial(\mathscr{A} \oplus \mathscr{B})$.

The membership test is based [54] on the alternative definition

$$\mathscr{A} \oplus \mathscr{B} = \{\mathbf{z} \,|\, \mathscr{A} \cap (-\mathscr{B} + \mathbf{z}) \neq \emptyset\}, \tag{9}$$

of a Minkowski sum, where the negation of a set $\mathscr{X}$ is simply

$$-\mathscr{X} = \{-\mathbf{x} \,|\, \mathbf{x} \in \mathscr{X}\}.$$

To verify this, note that $\mathbf{z} \in \mathscr{A} \oplus \mathscr{B} \iff \mathbf{z} \in \mathscr{B} + \mathbf{a}$ for some $\mathbf{a} \in \mathscr{A}$, which is equivalent $\mathbf{z} - \mathbf{a} \in \mathscr{B}$ or $\mathbf{a} - \mathbf{z} \in -\mathscr{B}$. Writing the latter as $\mathbf{a} \in -\mathscr{B} + \mathbf{z}$, we infer that $\mathbf{z} \in \mathscr{A} \oplus \mathscr{B} \iff \mathscr{A} \cap (-\mathscr{B} + \mathbf{z}) \neq \emptyset$. Definition (9) allows us to transform the question of point membership (for a representative point in the interior of each "face" delineated by the set of envelope segments) into the problem of whether two sets have a null intersection, which can be solved for sets bounded by parametric curves by standard numerical methods.

[5] The curve derivatives satisfy $\boldsymbol{\alpha}'(u) \neq 0$ for $u \in [0, 1]$ and $\boldsymbol{\beta}'(v) \neq 0$ for $v \in [0, 1]$.

Since the superset of $\partial(\mathscr{A} \oplus \mathscr{B})$ on the right-hand side of (8) often exhibits many "interior" segments, that do not belong to the true Minkowski sum boundary, the generate-and-test paradigm is computationally very wasteful. Extensive geometrical calculations and approximations must be performed, only to have their outcomes subsequently discarded, based on the result of an expensive membership test. It seems natural, therefore, to seek new methods that are designed to minimize the amount of "unnecessary" intermediate computations performed in evaluating $\partial(\mathscr{A} \oplus \mathscr{B})$.

A first step in this direction was reported in [34]: when the set boundaries $\partial\mathscr{A}$ and $\partial\mathscr{B}$ are described by regular parameterizations $\boldsymbol{\alpha}(u)$, $u \in [0, 1]$ and $\boldsymbol{\beta}(v)$, $v \in [0, 1]$ the condition $\mathbf{t}_a = \pm\mathbf{t}_b$ that identifies corresponding points $\mathbf{a} \in \partial\mathscr{A}$, $\mathbf{b} \in \partial\mathscr{B}$ can be interpreted as defining an implicit curve $F(u, v) = 0$ on the domain $(u, v) \in [0, 1]^2$—periodic with respect to the two variables, since $\boldsymbol{\alpha}(u)$, $\boldsymbol{\beta}(v)$ are smooth closed curves. By determining the topological structure of $F(u, v) = 0$ on this domain, using the *curve description algorithm* [48] based on Morse theory, one can identify a priori corresponding intervals in u, v that satisfy the matching criterion but cannot contribute to $\partial(\mathscr{A} \oplus \mathscr{B})$, and can thus be disqualified from consideration without additional work.

This paper presents a new algorithm that achieves further improvements in efficiency of Minkowski sum boundary evaluations by giving priority in the early stages to topological considerations, and deferring detailed geometrical approximations until *after* all the extraneous "interior" envelope edges have been identified and discarded. The algorithm employs a decomposition of the Minkowski sum envelope into *monotone segments*—i.e., smooth segments along which the x and y coordinates vary monotonically. Thus, the output depends upon the orientation of the chosen coordinate axes (as is typical of such algorithms). Some key features of the new algorithm are:

1. It computes a planar graph that is isotopic to the envelope curve. The vertices of this graph correspond to certain "characteristic points" such as turning points and singular points, and the edges are in one-to-one correspondence with a set of monotone segments of the envelope curve.
2. Each face of the graph is assigned a degree, indicating the number of different ways its points arise as sums of pairs of points on $\partial\mathscr{A}$ and $\partial\mathscr{B}$. Graph edges that separate adjacent faces of zero and non-zero degree identify true Minkowski-sum boundary segments. Edges that separate adjacent faces of positive degree identify "internal" envelope segments.
3. If only the Minkowski sum boundary is desired, all internal edges may be discarded without further computation and the remaining monotone boundary segments are then approximated to a specified tolerance. In applications where the Minkowski sum "internal structure" is also of interest, the envelope segments corresponding to internal edges may be approximated geometrically, furnishing a comprehensive description of the multiplicity of coverage of $\mathscr{A} \oplus \mathscr{B}$ by the points of $\partial\mathscr{A}$, $\partial\mathscr{B}$.
4. The *curve description algorithm* plays a key role in the Minkowski sum computation. This algorithm has been proved [48] to yield topologically correct results under clearly stated assumptions. Unlike methods based on ad hoc approximations, there is no doubt concerning the topological correctness of the Minkowski sum boundary.

The following example [39] shows that even "simple" initial curves incur intricate structures in their Minkowski sum envelopes, and the variation of covering degree within the Minkowski sum. Moreover, this structure can be very sensitive to seemingly innocuous changes, such as a uniform scaling of one or both of the initial curves.

Example 1. Consider the Minkowski sum of the unit circle and the curve $y = x^4$, with the parameterizations $\mathbf{c}(\theta) = (\cos\theta, \sin\theta)$ for $0 \leqslant \theta < 2\pi$ and $\mathbf{r}(t) = (t, t^4)$ for $-\infty < t < +\infty$. The envelope is the *offset curve* at distance 1 from $\mathbf{r}(t)$, defined [39] in terms of its unit normal $\mathbf{n}(t)$ by

$$\mathbf{r}_1(t) = \mathbf{r}(t) \pm \mathbf{n}(t) \quad \text{with} \quad \mathbf{n}(t) = \frac{(-4t^3, 1)}{\sqrt{16t^6 + 1}}.$$

The five-point star apparent in Fig. 3 indicates that even "simple" curves yield complicated topological structures in their Minkowski sum envelopes. The origin of this structure can be understood [39] as follows. The curvature $\kappa(t) = 12t^2/(16t^6 + 1)^{3/2}$ of $\mathbf{r}(t)$ has maxima at $t = \pm 1/\sqrt[6]{56}$, corresponding to minimum radii of curvature $\rho_{\min} = 1/\kappa_{\max} = 9/14\sqrt[6]{7}$. When $d < \rho_{\min}$, the offset curves on both sides of $\mathbf{r}(t)$ are smooth. However, when $d = \rho_{\min}$, the "interior" offset develops two tangent-continuous points of infinite curvature corresponding to $t = \pm 1/\sqrt[6]{56}$, and as d continues to increase these points evolve into *swallowtail* structures [18], characterized by a pair of cusps and a

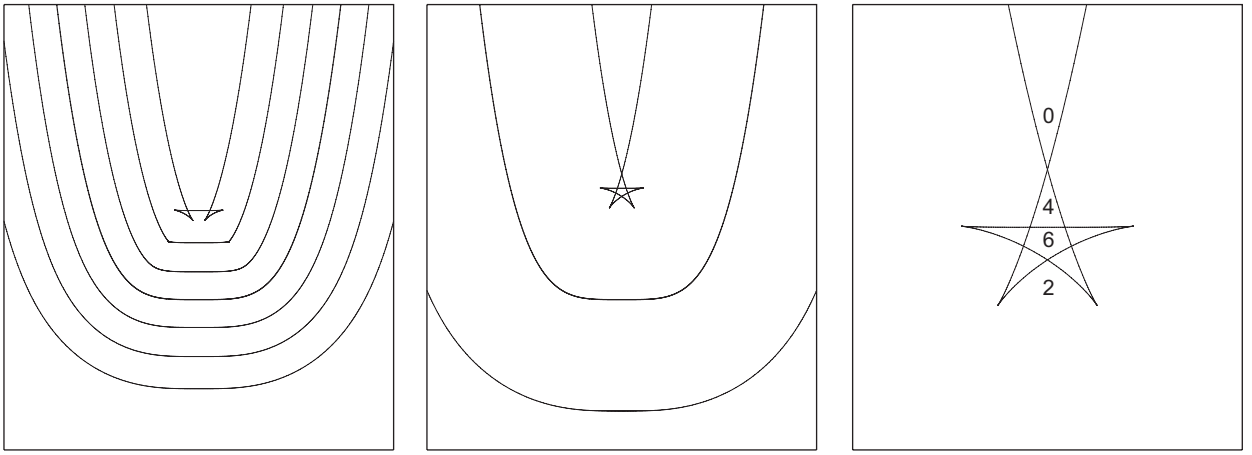

Fig. 3. Offsets to the curve $y = x^4$. Left: the interior offsets are smooth for $d < \rho_{\min}$, but develop points of infinite curvature at $d = \rho_{\min}$ that evolve into "swallowtails" for $d > \rho_{\min}$. Center: when $d = 1$, the overlap of the two swallowtails yields a five-point star. Right: enlargement showing the degree of covering along the symmetry axis. The exterior offsets are always smooth.

self-intersection (the cusps correspond to points where $\kappa(t) = 1/d$). Finally, when $d = 1$, the five-point star arises from an overlap of the two swallowtails.

This example appropriately illustrates how the *degree* of the Minkowski sum covering varies between the regions delineated by the envelope. Consider how points on the symmetry axis $x = 0$ arise as sums of points $\mathbf{c}(\theta) + \mathbf{r}(t)$. Writing

$$x = \cos\theta + t, \quad y = \sin\theta + t^4,$$

substituting $\sin\theta = \pm\sqrt{1 - \cos^2\theta} = \pm\sqrt{1 - t^2}$ from the condition $x = 0$ into the equation for y, and squaring to remove the radical, yields

$$t^8 - 2yt^4 + t^2 + y^2 - 1 = 0. \tag{10}$$

This quartic in t^2 identifies the points on the curve $\mathbf{r}(t)$ whose sums with a point of $\mathbf{c}(\theta)$ yield a given Minkowski sum point $(0, y)$. We wish to determine, as a function of y, the number of distinct real roots t of this equation. When $y < 0$, *Descartes' Law of Signs* [82] suffices to determine this number. For $-\infty < y < -1$, the $t^8, t^6, t^4, t^2, 1$ coefficients have signs $+0++-+$. Since there are no sign changes, Eq. (10) has no positive roots for t^2, and the covering is thus of degree 0. For $-1 < y < 0$, however, the signature becomes $+0++-$, indicating exactly one positive root for t^2, and hence two equal and opposite t values. The covering is thus of degree 2 over this interval.

When $y > 0$ there are two or more coefficient sign changes and Descartes' Law does not offer a complete description. Consider the *discriminant* equation

$$y^3 - y^2 - \tfrac{9}{8}y + \tfrac{283}{256} = 0, \tag{11}$$

obtained by eliminating t^2 from Eq. (10) and its derivative with respect to t^2. The roots of (11) identify y values where the number of real roots t^2 of (10) may change. This equation has one negative and two positive roots: we are concerned only with the latter, which may be expressed as

$$y_2 = \tfrac{1}{3} + \sqrt{\tfrac{35}{18}}\cos\phi, \quad y_0 = \tfrac{1}{3} + \sqrt{\tfrac{35}{18}}\cos(\phi + 4\pi/3),$$

where, taking $0 \leqslant 3\phi < \pi$, the angle ϕ is defined[6] by

$$\cos 3\phi = -\tfrac{4537}{560\sqrt{70}} \approx -0.9683.$$

[6] We employ here the trigonometric solution [82] to the cubic equation (11), since it has a negative discriminant.

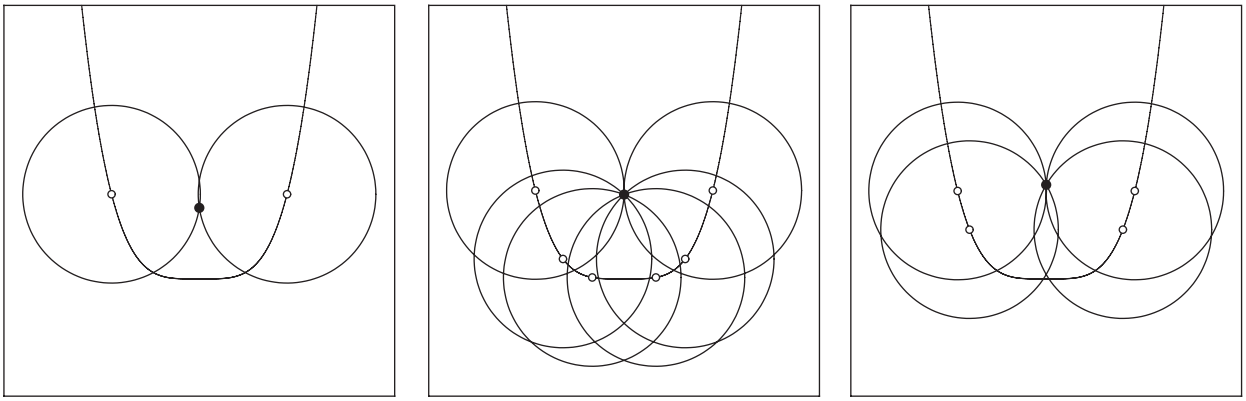

Fig. 4. Generation of representative points $(0, y)$ on the symmetry axis of the Minkowski sum in Fig. 3. Left: 2-fold generation of a point below the star. Center: 6-fold generation of a point within the pentagonal "core" of the star. Right: 4-fold generation of a point in the upward arm of the star.

The approximate numerical values are $y_0 \approx 0.9267$, $y_2 \approx 1.1295$. Augmenting these roots with the value $y_1 = 1$, at which (10) evidently has the double root $t = 0$, the qualitative root behavior may be summarized as follows:

1. When $0 < y < y_0$, Eq. (10) has exactly one positive real root t^2, identifying one pair of equal and opposite t values that generate points $(0, y)$ of the Minkowski sum. This identifies the region below the star, which thus has degree 2 covering.
2. When $y_0 < y < y_1$, Eq. (10) has exactly three positive real roots t^2, each identifying a pair of equal and opposite t values that generate the Minkowski sum point $(0, y)$. This interval identifies the pentagonal "core" of the star, which thus has degree 6 covering.
3. When $y_1 < y < y_2$, Eq. (10) has exactly two positive real roots t^2, each identifying a pair of equal and opposite t values that generate the Minkowski sum point $(0, y)$. This interval identifies the upward arm of the star, which thus has degree 4 covering.
4. When $y > y_2$, Eq. (10) has no positive real roots, and points $(0, y)$ have degree 0 covering—i.e., they lie outside the Minkowski sum.

The four other arms of the star can also be shown to have degree 4 coverings. Fig. 4 shows how representative points on the symmetry axis arise through distinct positions of the circle $\mathbf{c}(\theta)$.

The algorithm presented here gives information beyond the nominal set of points in the Minkowski sum of two curves: it also determines the *degree* of each point in the plane, i.e., the number of times it occurs as a sum of different pairs of points from $\boldsymbol{\alpha}(u)$ and $\boldsymbol{\beta}(v)$. The defining property of the Minkowski sum boundary is that the degree changes from zero to a positive integer as one crosses the boundary. Information on the degree can be useful in path planning, manufacturing, inspection, and similar applications. For example, *stereolithography* and *selective laser sintering* are two "rapid prototyping" technologies that involve, respectively, curing of photopolymers and fusing of powdered materials by exposure to a laser beam. The amount of exposure of a given area can be described in terms of the Minkowski sum of the beam cross-section with its center-line path. Information on the degree can thus be employed to minimize under/over-exposure in the path planning process.

Remark 1. Since efficient algorithms for computing the Minkowski sums of plane polygons are available [2,49,54] one can, in principle, approximate the Minkowski sum of analytic curves by first approximating them with polygons and applying these algorithms. However, it is difficult to guarantee a priori polygonal approximations that are sufficiently accurate to ensure an outcome topologically equivalent to the exact Minkowski sum. Fig. 5 illustrates this problem in the context of the offset to the curve $y = x^4$—see Example 1.

While insufficiently fine polygonal approximations can yield topologically incorrect results, fine approximations incur high computational costs. The algorithm proposed below circumvents these problems, with a computational cost that is determined primarily by the complexity of the final result.

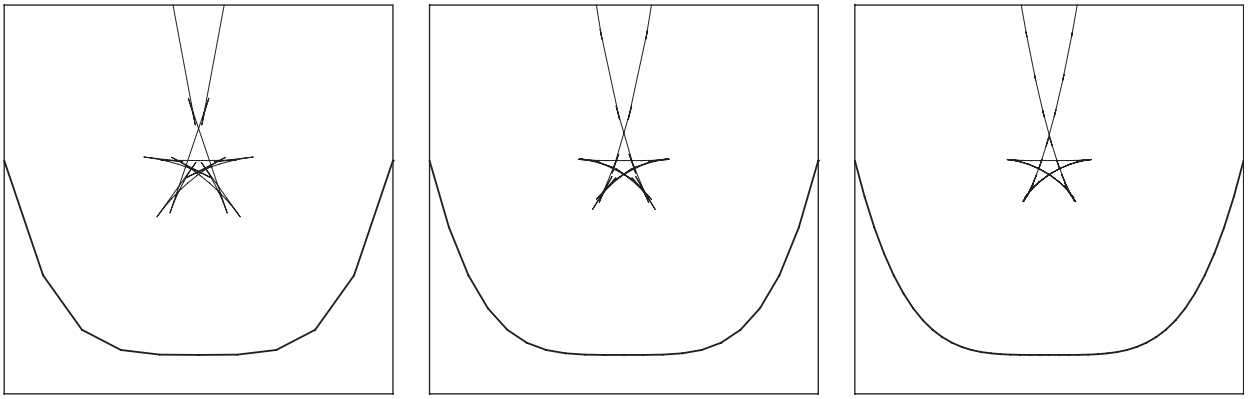

Fig. 5. Interior offsets at distance $d = 1$ to polygonal approximations of the curve $\mathbf{r}(t) = (t, t^4)$ defined by sampling with the parameter increments $\Delta t = 0.2, 0.1, 0.05$—compare with the exact offset curve shown in Fig. 3.

4. Minkowski sum envelope curves

We now study the geometry of the boundary of a Minkowski sum $\boldsymbol{\alpha}(u) \oplus \boldsymbol{\beta}(v)$ of two closed C^2 curves, defined on $u, v \in [0, 1]$. The extension to bounded (i.e., non-closed) curves will be discussed below. The Minkowski sums of very general closed sets can be realized as limits of sums of regions bounded by generic smooth curves. First, we give a lemma that helps simplify subsequent computations. For intrinsic properties such as smoothness or curvature, that are invariant under translation, this lemma allows us to position the curves so their Minkowski sum is especially easy to analyze.

Lemma 1. *Let* $\boldsymbol{\alpha}_{\mathbf{p}}(u) = \boldsymbol{\alpha}(u) + \mathbf{p}$ *be the translate of* $\boldsymbol{\alpha}(u)$ *by a point* $\mathbf{p} \in \mathbb{R}^2$. *Then the Minkowski sum* $\boldsymbol{\alpha}_{\mathbf{p}}(u) \oplus \boldsymbol{\beta}(v)$ *is equal to* $\boldsymbol{\alpha}(u) \oplus \boldsymbol{\beta}(v) \oplus \{\mathbf{p}\}$.

Proof. Both sets coincide with the points $\boldsymbol{\alpha}(u) + \boldsymbol{\beta}(v) + \mathbf{p}$ for $u, v \in [0, 1]$. □

It is convenient to use the complex numbers $\mathbb{C}$ as a representation for $\mathbb{R}^2$. We express a point as either $x + \mathrm{i}y$ or (x, y) and write the curves in terms of components as $\boldsymbol{\alpha}(u) = p(u) + \mathrm{i}q(u)$, $\boldsymbol{\beta}(v) = r(v) + \mathrm{i}s(v)$. Associated with the Minkowski sum $\boldsymbol{\alpha}(u) \oplus \boldsymbol{\beta}(v)$ of closed curves is a map[7] $\mathbf{f} : S^1 \times S^1 \to \mathbb{C}$ defined by $\mathbf{f}(u, v) = \boldsymbol{\alpha}(u) + \boldsymbol{\beta}(v)$. The inverse function theorem states that, at points where the Jacobian of $\mathbf{f}$ is non-singular, this map is a local diffeomorphism, and in particular the image point is an interior point. Thus, all points on the boundary $\partial(\boldsymbol{\alpha}(u) \oplus \boldsymbol{\beta}(v))$ are *singular values* of this map, images of *singular points* at which the Jacobian matrix has zero determinant:

$$\det(J(u, v)) = \begin{vmatrix} p'(u) & r'(v) \\ q'(u) & s'(v) \end{vmatrix} = 0. \tag{12}$$

We denote the set of singular values of $\mathbf{f}$ in $\mathbb{C}$ by Γ, and refer to it as the "local boundary" or *envelope* of $\boldsymbol{\alpha}(u) \oplus \boldsymbol{\beta}(v)$:

$$\Gamma = \{\mathbf{z} \in \mathbb{C} : \mathbf{z} = \boldsymbol{\alpha}(u) + \boldsymbol{\beta}(v) \text{ and } \det(J(u, v)) = 0\}.$$

The notion of an envelope was introduced in Section 2. The alternative name "local boundary" reflects the fact that, while portions of Γ can lie within the interior of $\boldsymbol{\alpha}(u) \oplus \boldsymbol{\beta}(v)$, all points on Γ form part of the boundary of the Minkowski sum of certain open subsegments of $\boldsymbol{\alpha}(u)$ and $\boldsymbol{\beta}(v)$.

[7] Here S^1 denotes the unit circle. Analogous maps $\mathbf{f} : I \times S^1 \to \mathbb{C}$ or $I \times I \to \mathbb{C}$ exist when one or both curves is a bounded arc defined on $I = [0, 1]$. For brevity, we confine our attention at present to closed curves.

We require $\boldsymbol{\alpha}(u)$ and $\boldsymbol{\beta}(v)$ to be sufficiently regular to avoid the possibility of infinitely many self-intersections of the envelope Γ. A sufficient condition for this is that $\boldsymbol{\alpha}(u)$ and $\boldsymbol{\beta}(v)$ are both piecewise-analytic—i.e., they consist of a finite number of segments with analytic parameterizations. A sum of two analytic curves is also analytic, and analytic curves have finitely many self-intersections. In practical applications, $\boldsymbol{\alpha}(u)$ and $\boldsymbol{\beta}(v)$ are often piecewise-algebraic, and therefore satisfy this condition.

Lemma 2. *For regular curves $\boldsymbol{\alpha}(u)$, $\boldsymbol{\beta}(v)$ the tangent vectors $\boldsymbol{\alpha}'(u)$, $\boldsymbol{\beta}'(v)$ are parallel if and only if (u, v) is a singular point of* $\mathbf{f}$.

Proof. At a singular point of $\mathbf{f}$, satisfaction of the Jacobian condition (12) is equivalent to parallelism of $\boldsymbol{\alpha}'(u) = (p'(u), q'(u))$, $\boldsymbol{\beta}'(v) = (r'(v), s'(v))$. □

It follows that Γ consists of sums of points on $\boldsymbol{\alpha}(u)$ and $\boldsymbol{\beta}(v)$ with parallel tangent vectors,

$$\Gamma = \{\boldsymbol{\alpha}(u) + \boldsymbol{\beta}(v) : \boldsymbol{\alpha}'(u) \parallel \boldsymbol{\beta}'(v)\}.$$

We now introduce the notion of a "generic" pair of curves. To each point of a plane curve $\boldsymbol{\alpha}(u)$ we may associate [21] a tangent vector $\mathbf{t}(u)$ and a curvature vector $\mathbf{k}(u)$, defined by

$$\mathbf{t}(u) = \frac{\boldsymbol{\alpha}'(u)}{|\boldsymbol{\alpha}'(u)|}, \quad \mathbf{k}(u) = \frac{1}{|\boldsymbol{\alpha}'(u)|^2}\left[\boldsymbol{\alpha}''(u) - \frac{\boldsymbol{\alpha}'(u)\cdot\boldsymbol{\alpha}''(u)}{|\boldsymbol{\alpha}'(u)|^2}\boldsymbol{\alpha}'(u)\right].$$

If $\boldsymbol{\alpha}(u)$ is parameterized by arc length, $\mathbf{t}(u) = \boldsymbol{\alpha}'(u)$ and $\mathbf{k}(u) = \boldsymbol{\alpha}''(u)$. The curvature vector points toward the center of curvature of the curve $\boldsymbol{\alpha}(u)$, and is independent of its parameterization or orientation. Let $\mathbf{t}(u)$, $\mathbf{t}(v)$ be the tangent vectors and $\mathbf{k}(u)$, $\mathbf{k}(v)$ be the curvature vectors of $\boldsymbol{\alpha}(u)$, $\boldsymbol{\beta}(v)$.

Definition 1. A pair of curves $\boldsymbol{\alpha}(u)$ and $\boldsymbol{\beta}(v)$ is *generic* when:
1. $\boldsymbol{\alpha}(u)$, $\boldsymbol{\beta}(v)$ are regularly parameterized C^2 curves, with continuous second derivatives and non-vanishing first derivatives;
2. $\boldsymbol{\alpha}(u)$, $\boldsymbol{\beta}(v)$ each have finitely many points of zero curvature;
3. there are finitely many pairs of points where $\mathbf{k}(u) + \mathbf{k}(v) = 0$.

Generic curves can be segmented into finitely many arcs along which the curvature is of constant sign—namely, the arcs between isolated zeros of the curvature. Most pairs of curves are generic, in the sense that generic curves form an open dense subset of the space of all curve pairs.

Example 2. When $\boldsymbol{\alpha}(u)$ is a circle of radius d and $\boldsymbol{\beta}(v)$ is a general curve, the Minkowski sum boundary $\partial(\boldsymbol{\alpha}(u) \oplus \boldsymbol{\beta}(v))$ is the *offset curve* [39] at distance $\pm d$ from $\boldsymbol{\beta}(v)$. The Minkowski sum is the set of points in a "tubular region" of width $2d$ about $\boldsymbol{\beta}(v)$. If $\boldsymbol{\beta}(v)$ is a circle of radius $\delta < d$, $\boldsymbol{\alpha}(u) \oplus \boldsymbol{\beta}(v)$ is an annulus with inner and outer radii $d - \delta$ and $d + \delta$. Such circle pairs are generic. If $\delta = d$, the inner boundary of the annulus degenerates to a point, a symptom of the fact that the curves are not generic. If $\delta > d$, the sum is again an annulus, with inner and outer radii $\delta - d$ and $\delta + d$. See Fig. 6.

Definition 2. The *self-intersections* of the envelope Γ are points generated by distinct pairs of parameter values $(u_1, v_1) \neq (u_2, v_2)$ such that

$$\boldsymbol{\alpha}(u_1) + \boldsymbol{\beta}(v_1) = \boldsymbol{\alpha}(u_2) + \boldsymbol{\beta}(v_2), \quad \boldsymbol{\alpha}'(u_1) \parallel \boldsymbol{\beta}'(v_1), \quad \boldsymbol{\alpha}'(u_2) \parallel \boldsymbol{\beta}'(v_2).$$

The first condition states that the pairs of points must have coincident sums, and the last two ensure that these sums yield points on the envelope Γ. In components, these amount to four scalar equations in four unknowns:

$$p(u_1) + r(v_1) = p(u_2) + r(v_2), \quad q(u_1) + s(v_1) = q(u_2) + s(v_2),$$

$$p'(u_1)s'(v_1) - r'(v_1)q'(u_1) = 0, \quad p'(u_2)s'(v_2) - r'(v_2)q'(u_2) = 0.$$

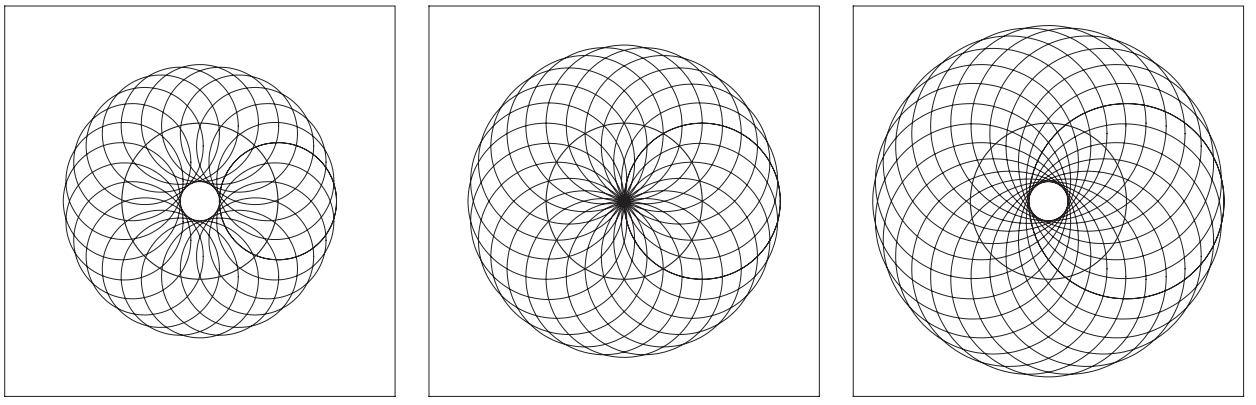

Fig. 6. Minkowski sum of circles of radii d and δ. Left: if $\delta < d$, the sum is a circular annulus. Center: if $\delta = d$, the genericity conditions are violated, and the inner boundary of the annulus degenerates to a point. Right: if $\delta > d$, the Minkowski sum is again a circular annulus.

Definition 3. *Non-regular points* of the envelope occur where $\boldsymbol{\alpha}(u) + \boldsymbol{\beta}(v)$ yields a point on Γ and: (i) one of the curvature vectors $\mathbf{k}(u)$, $\mathbf{k}(v)$ vanishes; or (ii) these vectors are non-vanishing, but their sum $\mathbf{k}(u) + \mathbf{k}(v)$ vanishes. They include "ordinary" cusps (i.e., tangent reversals) as well as higher-order singularities of the envelope tangent, and are identified by solving two scalar equations in u and v—namely, for case (i)

$$\boldsymbol{\alpha}'(u) \parallel \boldsymbol{\beta}'(v) \quad \text{and} \quad |\mathbf{k}(u)| = 0 \ \text{ or } \ |\mathbf{k}(v)| = 0,$$

and for case (ii) the x and y components of

$$\mathbf{k}(u) + \mathbf{k}(v) = 0.$$

This subsumes the condition $\boldsymbol{\alpha}'(u) \parallel \boldsymbol{\beta}'(v)$ for a point $\mathbf{c} = \boldsymbol{\alpha}(u) + \boldsymbol{\beta}(v)$ to lie on Γ since $\mathbf{k}(u)$, $\mathbf{k}(v)$ are orthogonal to $\boldsymbol{\alpha}'(u)$, $\boldsymbol{\beta}'(v)$. The generic case of a cusp occurs when $\mathbf{k}(u) + \mathbf{k}(v) = 0$ but $\mathbf{k}(u)$, $\mathbf{k}(v)$ are non-zero.

Lemma 3. *For a generic pair of curves, the Minkowski sum envelope Γ is a piecewise-smooth immersed curve that admits a regular parameterization in a neighborhood of each point except the self-intersections and non-regular points. If $\mathbf{c} = \boldsymbol{\alpha}(u_0) + \boldsymbol{\beta}(v_0) \in \Gamma$, then Γ is parallel at $\mathbf{c}$ to $\boldsymbol{\alpha}(u_0)$ and $\boldsymbol{\beta}(v_0)$.*

Proof. Suppose $\mathbf{c} = \boldsymbol{\alpha}(u_0) + \boldsymbol{\beta}(v_0) \in \Gamma$, so $\boldsymbol{\alpha}'(u_0) \parallel \boldsymbol{\beta}'(v_0)$, and assume that $\mathbf{k}(u_0)$, $\mathbf{k}(v_0)$, $\mathbf{k}(u_0) + \mathbf{k}(v_0)$ are all non-zero. We will show that the portion of Γ generated by taking a sum of neighborhoods of $\boldsymbol{\alpha}(u_0)$, $\boldsymbol{\beta}(v_0)$ is a smooth arc containing $\mathbf{c}$. To simplify the analysis, we reparameterize the curves so that $u_0 = v_0 = 0$, and choose coordinates such that both curves are tangent to the real axis at $\boldsymbol{\alpha}(0) = \boldsymbol{\beta}(0) = (0, 0)$. We are interested in the portion of Γ generated by open arcs of non-zero curvature around $\boldsymbol{\alpha}(0)$ and $\boldsymbol{\beta}(0)$. For sufficiently small arcs, we can assume that $\mathbf{k}(u)$, $\mathbf{k}(v)$, $\mathbf{k}(u) + \mathbf{k}(v)$ are all non-vanishing—we denote such arcs by $\bar{\boldsymbol{\alpha}}$ and $\bar{\boldsymbol{\beta}}$.

Now $\bar{\boldsymbol{\alpha}}$ and $\bar{\boldsymbol{\beta}}$ are both graphs over the x-axis in some neighborhood of the origin. Taylor series approximations of these graphs give $y = ax^2 + e_1(x)$ for $\bar{\boldsymbol{\alpha}}$ and $y = bx^2 + e_2(x)$ for $\bar{\boldsymbol{\beta}}$, where a and b are the (signed) curvatures of $\bar{\boldsymbol{\alpha}}$ and $\bar{\boldsymbol{\beta}}$ at the origin. Also, $e_1(x)$ and $e_2(x)$, being the difference of two C^2 functions with zero first and equal second derivatives at $x = 0$, are themselves C^2 functions with vanishing first and second derivatives at the origin.

Since $\bar{\boldsymbol{\alpha}}(u)$ has non-zero curvature at $u = 0$, its Gauss map $G_{\bar{\boldsymbol{\alpha}}}$ defines a differentiable one-to-one map from a neighborhood of $\bar{\boldsymbol{\alpha}}(0)$ to an arc of the unit circle, each curve point being mapped to the corresponding normal. Similarly for the Gauss map $G_{\bar{\boldsymbol{\beta}}}$ of $\bar{\boldsymbol{\beta}}$. Thus, each tangent of $\bar{\boldsymbol{\alpha}}$ sufficiently close to the origin is parallel to a unique tangent of $\bar{\boldsymbol{\beta}}$. Now let $(t, bt^2 + e_2(t))$ be the point on $\bar{\boldsymbol{\beta}}$ whose tangent is parallel to that of $\bar{\boldsymbol{\alpha}}(x)$ at $(x, ax^2 + e_1(x))$. Then $t = G_{\bar{\boldsymbol{\beta}}}^{-1} \circ G_{\bar{\boldsymbol{\alpha}}}$ is a differentiable function of x, with $t(0) = 0$. Moreover, since the curvature is proportional to the derivative of the Gauss map, the non-zero curvatures of $\bar{\boldsymbol{\alpha}}$ and $\bar{\boldsymbol{\beta}}$ at the origin ensure that $t'(0) \neq 0$.

The two tangents are parallel at points on the graphs in the (x, y) plane that exhibit equal slopes. Equating the slope of $\bar{\boldsymbol{\alpha}}$ at $(x, ax^2 + e_1(x))$ to the slope of $\bar{\boldsymbol{\beta}}$ at $(t, bt^2 + e_2(t))$ yields

$$2ax + \frac{\mathrm{d}e_1}{\mathrm{d}x} = 2bt + \frac{\mathrm{d}e_2}{\mathrm{d}t},$$

which may be solved for t to obtain

$$t = \frac{a}{b}x + \frac{1}{2b}\left[\frac{\mathrm{d}e_1}{\mathrm{d}x} - \frac{\mathrm{d}e_2}{\mathrm{d}t}\right].$$

To express the right-hand side as a function of x only, we use the chain rule

$$\frac{\mathrm{d}e_2}{\mathrm{d}x} = \frac{\mathrm{d}t}{\mathrm{d}x}\frac{\mathrm{d}e_2}{\mathrm{d}t}$$

to convert the derivative of e_2 with respect to t into a derivative with respect to x. Using primes to denote derivatives with respect to x, we then have

$$t = \frac{a}{b}x + \frac{1}{2b}\left[e_1' - \frac{e_2'}{t'}\right]. \tag{13}$$

Since the derivative t' appears on the right, this is an "implicit" definition of the function $t(x)$. Note that, for $\mathrm{d}e_2/\mathrm{d}t = e_2'/t'$ to be defined at $t = 0$, we must have $t'(0) \neq 0$.

Let $\bar{\Gamma}$ denote the subset of Γ arising from sums of points in $\bar{\boldsymbol{\alpha}}$ and $\bar{\boldsymbol{\beta}}$. We will show that $\bar{\Gamma}$ is a curve with non-zero derivative near the origin, and is thus regular at that point. In a neighborhood of $x = 0$, we can parameterize $\bar{\Gamma}$ in terms of x by summing points with parallel tangents to obtain

$$\bar{\boldsymbol{\gamma}}(x) = (x + t(x), ax^2 + bt^2(x) + e_1(x) + e_2(t(x))).$$

Substituting from (13), the derivative of $\bar{\boldsymbol{\gamma}}(x)$ can then be expressed as

$$\bar{\boldsymbol{\gamma}}'(x) = \left(1 + \frac{a}{b} + \frac{1}{2b}\left[e_1'' - \frac{t'e_2'' - t''e_2'}{t'^2}\right], 2ax + 2btt' + e_1' + e_2'\right),$$

and since $e_1' = e_1'' = 0$, $e_2' = e_2'' = 0$, $t = 0$ when $x = 0$, we have

$$\bar{\boldsymbol{\gamma}}'(0) = (1 + a/b, 0).$$

Since the condition $\mathbf{k}(u) + \mathbf{k}(v) \neq 0$ implies that $1 + a/b \neq 0$, we may conclude that in a neighborhood of the origin $\bar{\boldsymbol{\gamma}}$ coincides with a non-singular curve, whose tangent at the origin is parallel to that of $\bar{\boldsymbol{\alpha}}$ and $\bar{\boldsymbol{\beta}}$. □

Corollary 1. *For a generic pair of curves, Γ is a union of a finite number of regular curve segments.*

The envelope for the Minkowski sum of generic curves $\boldsymbol{\alpha}(u)$ and $\boldsymbol{\beta}(v)$ is a piecewise-smooth curve Γ that, in general, comprises a superset of the true boundary $\partial(\boldsymbol{\alpha}(u) \oplus \boldsymbol{\beta}(v))$. Typically, Γ also contains segments that lie within the *interior* of $\boldsymbol{\alpha}(u) \oplus \boldsymbol{\beta}(v)$. These "interior" segments of Γ also possess a geometrical significance, and can be identified by the nature of the change in the degree of $\mathbf{f}$ across them.

Lemma 4. *At a point $\mathbf{c} = \boldsymbol{\alpha}(u_0) + \boldsymbol{\beta}(v_0) \in \Gamma$ that is regular and not a self-intersection, there are short subarcs $\bar{\boldsymbol{\alpha}}$ and $\bar{\boldsymbol{\beta}}$ containing $\boldsymbol{\alpha}(u_0)$ and $\boldsymbol{\beta}(v_0)$, such that all points of the Minkowski sum $\bar{\boldsymbol{\alpha}} \oplus \bar{\boldsymbol{\beta}}$ lie on one side of $\bar{\boldsymbol{\gamma}}$ near $\mathbf{c}$, where $\bar{\boldsymbol{\gamma}} = \bar{\boldsymbol{\alpha}} \oplus \bar{\boldsymbol{\beta}}$. The side that contains the sum is the one for which the unit normal $\mathbf{n}$ to $\bar{\boldsymbol{\gamma}}$ at $\mathbf{c}$ has a positive dot product with the vector $\mathbf{k}(u_0) + \mathbf{k}(v_0)$.*

Proof. As in Lemma 3 we adopt coordinates so that $\bar{\boldsymbol{\alpha}}$ and $\bar{\boldsymbol{\beta}}$ coincide, in a neighborhood of the origin, with graphs $y = ax^2 + e_1(x)$ and $y = bx^2 + e_2(x)$. The (signed) curvatures of $\bar{\boldsymbol{\alpha}}$ and $\bar{\boldsymbol{\beta}}$ at the origin are a and b, and $a + b \neq 0$ by assumption. Consider first the case $a + b > 0$. We will show that interior points of $\bar{\boldsymbol{\alpha}} \oplus \bar{\boldsymbol{\beta}}$ lie above the curve $\bar{\boldsymbol{\gamma}}$.

To do this, it suffices to consider points along the y-axis, since the normal to any other point on $\bar{\boldsymbol{\alpha}} \oplus \bar{\boldsymbol{\beta}}$ can be moved so as to coincide with the y-axis. Suppose $(x, ax^2 + e_1(x))$ and $(w, bw^2 + e_2(w))$ sum to a point $(0, y_0)$. Then $x = -w$ and $y_0 = (a+b)x^2 + e_1(x) + e_2(-x)$. This sum is positive for x sufficiently small, since e_1 and e_2 have zero first and second derivatives at $x = 0$, and by L'Hôpital's rule we thus have

$$\lim_{x\to 0} \frac{1}{x^2}[(a+b)x^2 + e_1(x) + e_2(-x)] = a + b > 0.$$

Thus, the contribution to the sum $\bar{\boldsymbol{\alpha}} \oplus \bar{\boldsymbol{\beta}}$ lies on the side of $\bar{\boldsymbol{\gamma}}$ indicated by the vector $\mathbf{k}(u) + \mathbf{k}(v)$. A similar argument holds when $a + b < 0$. □

Lemma 5. *Crossing the envelope at a uniquely generated regular point* $\mathbf{c} = \boldsymbol{\alpha}(u_0) + \boldsymbol{\beta}(v_0) \in \Gamma$ *induces a change in the degree of* $\boldsymbol{\alpha}(u) \oplus \boldsymbol{\beta}(v)$ *by* ± 2. *On crossing* Γ *at* $\mathbf{c}$ *in the direction of the vector* $\mathbf{n}$, *the change in degree is*

$$\Delta = 2\,\mathrm{sign}[(\mathbf{k}(u_0) + \mathbf{k}(v_0)) \cdot \mathbf{n}]. \tag{14}$$

Proof. For x sufficiently close to 0, pairs of points $(x, ax^2 + e_1(x)) \in \bar{\boldsymbol{\alpha}}$ and $(-x, bx^2 + e_2(-x)) \in \bar{\boldsymbol{\beta}}$ sum to a point on the positive y-axis when $a + b > 0$. We will show that each point of the positive y-axis in a small neighborhood of (0,0) is realized as such a sum in precisely two ways.

Consider the sum $y = (a+b)x^2 + e_1(x) + e_2(-x)$ of the y coordinates of two such points as a function of x. We show that this function has a non-zero derivative y' in a deleted neighborhood of $x = 0$. The derivative is

$$y' = 2(a+b)x + e_1'(x) + e_2'(-x),$$

and since $e_1(x)$ and $e_2(x)$ have zero first and second derivatives at $x = 0$, for small $|x|$ we have by L'Hôpital's rule

$$\lim_{x\to 0} \frac{1}{x}[2(a+b)x + e_1'(x) + e_2'(-x)] = 2(a+b) > 0.$$

This implies that, for $|x|$ sufficiently small, $y' > 0$ for $x > 0$ and $y' < 0$ for $x < 0$. Specifically, small intervals on each side of $x = 0$ map one-to-one to a small interval of the y-axis above the origin. Thus, for sufficiently small δ, points $(0, y)$ with $0 < y < \delta$ occur precisely twice in the Minkowski sum as a result of adding points from $\bar{\boldsymbol{\alpha}}$ and $\bar{\boldsymbol{\beta}}$. The case $a + b < 0$ is identical, except that the sum yields points on the negative y-axis.

Since $\mathbf{k}(u_0) + \mathbf{k}(v_0) \neq 0$ (because $\mathbf{c}$ is assumed to be a regular point of Γ), the change in degree upon crossing Γ in the direction of a vector $\mathbf{n}$ is given by expression (14) for both the cases $a + b > 0$ and $a + b < 0$. □

In Lemma 5 we assume that $\mathbf{c}$ is *uniquely* generated on Γ as the sum of points on $\boldsymbol{\alpha}(u)$ and $\boldsymbol{\beta}(v)$. If other, distinct pairs of points on $\boldsymbol{\alpha}(u)$ and $\boldsymbol{\beta}(v)$ also generate $\mathbf{c}$, they will also incur a change in the degree of the covering by ± 2 upon crossing Γ at $\mathbf{c}$. Thus, in the most general context, crossing the envelope curve always incurs a change in the degree by a multiple of 2.

Lemma 6. *The covering degree is constant in each of the connected regions comprising the complement of the envelope curve* Γ.

Proof. In the complement of Γ, the map $\mathbf{f}(u, v) = \boldsymbol{\alpha}(u) + \boldsymbol{\beta}(v)$ has non-zero Jacobian, and is therefore a local diffeomorphism. Hence, the number of pre-image points does not change in a complementary region. □

We can determine the degree of each region in the complement of Γ by using formula (14), that describes how the degree changes as we move across a segment of Γ. To compute the degree of an arbitrary point $\mathbf{p}$, we connect it to infinity by a line that crosses Γ transversely at finitely many regular points. Beginning with degree zero, we increment the degree by ± 2 each time we cross Γ, in accordance with Lemma 5.

5. Characteristic points of the envelope

In Section 6 we present an algorithm that determines the structure of the envelope Γ via Morse Theory [69], using an analysis of its local extrema in two directions. For any unit vector $\mathbf{n}$ we define a height function on $\mathbb{R}^2$ by $h_{\mathbf{n}}(\mathbf{z}) = \mathbf{n} \cdot \mathbf{z}$.

The *critical points* of Γ with respect to $h_{\mathbf{n}}(\mathbf{z})$ are the local extrema of this function, restricted to Γ—they can be identified by solving certain equations.

Lemma 7. *The critical points of Γ with respect to a height function $h_{\mathbf{n}}$ are its regular points satisfying*

$$\{\mathbf{c} = \boldsymbol{\alpha}(u) + \boldsymbol{\beta}(v) : \mathbf{n} \cdot \boldsymbol{\alpha}'(u) = \mathbf{n} \cdot \boldsymbol{\beta}'(v) = 0\}.$$

Proof. Suppose that $\mathbf{c} = \boldsymbol{\alpha}(u) + \boldsymbol{\beta}(v)$ is a non-singular point of Γ. Then by Lemma 3, $\boldsymbol{\alpha}'(u) = (p'(u), q'(u))$ is parallel to $\boldsymbol{\beta}'(v) = (r'(v), s'(v))$, and Γ is parallel to both at $\mathbf{c}$. Thus, if Γ is normal to $\mathbf{n}$ at $\mathbf{c}$ then it is a sum of two points each of which is also normal to $\mathbf{n}$. □

Definition 4. The *turning points* of the envelope Γ are those points where its tangent is horizontal or vertical. They are identified by solving the system of equations

$$\mathbf{n} \cdot \boldsymbol{\alpha}'(u) = \mathbf{n} \cdot \boldsymbol{\beta}'(v) = 0$$

in Lemma 7 with $\mathbf{n} = (1, 0)$ and $\mathbf{n} = (0, 1)$—these amount to two scalar equations in two unknowns.

Definition 5. For a bounded domain R, the *border points* of the envelope are the points of Γ on the boundary of R. If, for example, R is a rectangle, they can be identified by noting that the points $(p(u) + r(v), q(u) + s(v))$ of Γ on a line $ax + by = c$ satisfy the equations

$$a(p(u) + r(v)) + b(q(u) + s(v)) = c, \quad p'(u)s'(v) - r'(v)q'(u) = 0.$$

In order to employ the curve description algorithm [34] to recover Γ, we need to identify its *characteristic points* on a given domain R. These include its self-intersections (Definition 2) and non-regular points (Definition 3), its critical points with respect to two orthogonal directions (Definition 4)—we take $\mathbf{n} = (1, 0)$ and $(0, 1)$—and its points on the boundary of the domain R (Definition 5). We refer to the self-intersections and non-regular points of Γ collectively as its *singular points.*

6. Curve description algorithm

To analyze the structure of the Minkowski sum envelope curve, we employ the *curve description algorithm* developed in [48]. Given the characteristic points, as described in Section 5, and the ability to compute other envelope points lying on horizontal and vertical lines within rectangular subdomains, this algorithm generates a piecewise-linear graph $\mathcal{G}$ isotopic to the envelope curve Γ in a domain $R = [a, b] \times [c, d]$. The characteristic points of Γ are vertices of $\mathcal{G}$, and the edges of $\mathcal{G}$ correspond to monotone segments of Γ.

The curve description algorithm was motivated by specific requirements of surface perturbation schemes [81] that ensure topological consistency of the representations of free-form surface intersections, but it is broadly applicable to general problems concerned with the topological configuration of planar curves. The determination of basic shape information for a plane curves (i.e., the number and nature of its real components, and their spatial relations) has been addressed using the exact-arithmetic *cylindrical algebraic decomposition* method [5–8] and was subsequently studied by other authors, using both symbolic and "semi-numerical" methods [4,20,44,45,50,76,77].

We now briefly summarize the curve description algorithm—complete details may be found in [48]. We consider the envelope Γ within a rectangular domain R, and assume that $\boldsymbol{\alpha}(u)$ and $\boldsymbol{\beta}(v)$, and hence Γ, have finitely many points of zero curvature—in particular, they contain no linear components.

Curve description algorithm.

1. *Find all the characteristic* (*singular*, *turning*, *and border*) *points of Γ.*

2. *Divide R into vertical strips without interior characteristic points.* If $\{x_1, \ldots, x_N\}$ is the ordered set of *distinct* x coordinates of all turning and singular points of Γ with $a < x < b$, dissect R into $N + 1$ strips $R_1, \ldots, R_{N+1}$ along the vertical lines $x = x_1, \ldots, x = x_N$. Also find the additional intersections of Γ with these lines. Each strip R_i has known points of Γ on its left and right boundary, but their connectivity is not known: there may be many different ways to join them with monotone arcs. The correct connectivity is found in the next step.

3. *Determine connectivity of points on the boundary of each vertical strip.* The following process is repeated for each strip $R_1, \ldots, R_{N+1}$.

Let $c = y_0 < y_1 < \cdots < y_{n_i} < y_{n_i+1} = d$ be the sequence of *distinct* y coordinates of points of Γ on the interior of the left and right sides of R_i, at $x = x_i$ and x_{i+1}, augmented by the y coordinates of R. Subdivide R_i by the horizontal lines $y = h_j = \frac{1}{2}(y_j + y_{j+1})$ for $0 \leqslant j \leqslant n_i$, and let the sub-rectangle containing y_j be denoted by R_{ij}. Note that the left and right sides of R_{ij} each contain at most one point of Γ.

By computing the intersections of Γ with each of the horizontal lines $y = h_j$ in the vertical strip, and with certain intermediate vertical lines in each sub-rectangle R_{ij}, one can construct a polygonal graph that is isotopic to Γ within R_{ij}, and has the same points as Γ on the boundary of R_{ij} (see [48] for details of this construction).

The union of all the sub-rectangle graphs for $1 \leqslant j \leqslant n_i$ yields an overall graph γ_i in the vertical strip R_i consisting of polygonal arcs that are embedded and disjoint in the interior of the strip R_i. Each edge of γ_i is a sequence of edges in the sub-rectangles R_{ij} that defines a polygonal arc within R_i, beginning and ending at distinct sides of the boundary of this strip. A new graph $\tilde{\gamma}_i$ for R_i is formed by replacing each polygonal edge of γ_i by the line segment connecting its end-points.

4. Take the union $\mathcal{G} = \bigcup_{i=1}^{N+1} \tilde{\gamma}_i$ of the graphs for all the vertical strips.

5. Output the resulting set of vertices and connecting edges, along with any isolated vertices meeting no edges, as the graph $\mathcal{G}$.

The curve description algorithm has the following useful properties:

Theorem 1. *Assume a method exists to locate all the border, turning, and singular points of the Minkowski sum envelope Γ for (x, y) in a given rectangle R. Then the* curve description algorithm *constructs a polygonal curve $\mathcal{G}$ that is isotopic to Γ in R. The isotopy fixes the domain boundary ∂R, and leaves each turning point, border point, and singular point of Γ fixed. All vertices of $\mathcal{G}$ are points on Γ, and all turning points, border points, and singular points of Γ are located at vertices of $\mathcal{G}$.*

The proof, and complete details on the curve description algorithm, are given in [48]. The following example illustrates the operation of this algorithm.

Example 3. Consider again (as in Example 1) the curves $\mathbf{r}(t) = (t, t^4)$ and $\mathbf{c}(\theta) = (\cos\theta, \sin\theta)$. With $\mathbf{n} = (1, 0)$ the equations for vertical turning points have no solution. With $\mathbf{n} = (0, 1)$ the equations for horizontal turning points are $\cos\theta = 4t^3 = 0$, with solutions $\theta = \pi/2, t = 0$ and $\theta = 3\pi/2, t = 0$ that identify horizontal turning points at $(0, 1)$ and $(0, -1)$.

Self-intersections are identified by pairs of values (θ_1, t_1) and (θ_2, t_2) satisfying

$$\cos\theta_1 + t_1 = \cos\theta_2 + t_2, \quad \sin\theta_1 + t_1^4 = \sin\theta_2 + t_2^4,$$

$$\cos\theta_1 + 4t_1^3 \sin\theta_1 = 0, \quad \cos\theta_2 + 4t_2^3 \sin\theta_2 = 0.$$

For self-intersections on the symmetry axis $x = 0$, these equations may be reduced to a simple polynomial equation

$$16t^6 - 16t^4 + 1 = 0$$

in t^2. With $\cos 3\phi = \frac{5}{32}$, this has two positive real roots given by

$$t^2 = \tfrac{1}{3} + \tfrac{2}{3}\cos\phi \quad \text{and} \quad t^2 = \tfrac{1}{3} + \tfrac{2}{3}\cos(\phi + 4\pi/3),$$

which yield the approximate solutions $t = \pm 0.5463, \theta = \mp 0.9928, y = 0.9267$ and $t = \pm 0.9630, \theta = \mp 0.2730, y = 1.1295$.

For the other self-intersections, reduction to an equation in t alone yields a polynomial of high degree [39]. It is preferable to use the original equations, which may be solved robustly by coupling subdivision with Newton–Raphson iterations governed by the Kantorovich convergence test. The approximate coordinates of the remaining four self-intersections are

$$(\pm 0.0393, 1.0000) \quad \text{and} \quad (\pm 0.0540, 0.9575)$$

corresponding to the pairs of parameter values $t_1 = \mp 0.9097, t_2 = \pm 0.0396$ and $t_1 = \mp 0.8877, t_2 = \pm 0.4990$.

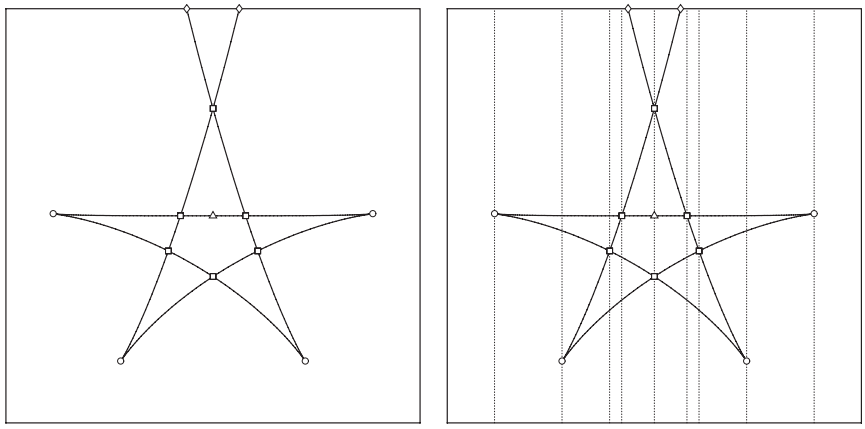

Fig. 7. Right: envelope characteristic points on $(x, y) \in [-\frac{1}{4}, \frac{1}{4}] \times [\frac{3}{4}, \frac{5}{4}]$. Turning points are indicated by triangles; self-intersections by squares; cusps by circles; and border points by diamonds. Left: subdivision of the envelope into monotone segments by vertical lines through each of the singular points.

The condition $\mathbf{k}(\theta) + \mathbf{k}(t) = \mathbf{0}$ for cusps yields the equations

$$\cos\theta = -\frac{48t^5}{(16t^6+1)^2} \quad \text{and} \quad \sin\theta = \frac{12t^2}{(16t^6+1)^2}. \tag{15}$$

Eliminating θ, we obtain the polynomial equation

$$(16t^6+1)(4096t^{18} + 768t^{12} + 48t^6 - 144t^4 + 1) = 0.$$

The first factor has no real roots, and Descartes' Law of Signs indicates that the second factor has at most two positive real roots for t^2. One can verify that two roots do indeed exist. They yield the approximate numerical values ± 0.2908 and ± 0.7317 for t, and corresponding θ values can be found from (15). We thus obtain a total of four (ordinary) cusps.

Finally, if we restrict our attention to the domain $(x, y) \in [-\frac{1}{4}, \frac{1}{4}] \times [\frac{3}{4}, \frac{5}{4}]$ there are just two border points at $(x, y) \approx (\pm 0.0317, 1.25)$. Fig. 7 shows the 13 characteristic points of the envelope identified in this manner, and the subdivision of the envelope into 28 monotone segments by vertical lines through the singular points (cusps and self-intersections). In the present case, it is not necessary to introduce further points on Γ in step 3 of the curve description algorithm, since the connectivity of the points on the vertical lines bounding each strip is immediately apparent. The piecewise-linear graph $\mathcal{G}$ thus contains 56 edges. If desired, some edges may be combined to obtain a more concise yet still topologically faithful description of Γ in the domain R.

7. Computing Minkowski sums

We now present an algorithm to compute the Minkowski sum $\boldsymbol{\alpha}(u) \oplus \boldsymbol{\beta}(v)$ of two closed C^2 curves in $\mathbb{R}^2$. The algorithm produces a graph structure that is isotopic to the Minkowski sum envelope curve, and each critical point of the envelope is precisely represented as a vertex of this graph. The graph edges identify monotone segments of the envelope, which may be approximated to any desired geometrical tolerance by the interpolation of data sampled from the exact envelope. Moreover, the algorithm associates with each face of the graph a degree indicating how many ways each point in a face arises as the sum $\boldsymbol{\alpha}(u) + \boldsymbol{\beta}(v)$ of distinct pairs of points on the two curves. The Minkowski sum boundary $\partial(\boldsymbol{\alpha}(u) \oplus \boldsymbol{\beta}(v))$ can be identified as the set of edges that separate faces of zero and non-zero degree.

The "internal structure" of the Minkowski sum—i.e., its segmentation into regions with associated covering degrees—may be of interest in its own right for certain applications. Even in applications where only the Minkowski sum boundary is desired, however, the algorithm offers significant efficiency improvements by minimizing geometrical computations performed on edges that do not contribute to the final boundary. The algorithm to compute the Minkowski sum $\boldsymbol{\alpha}(u) \oplus \boldsymbol{\beta}(v)$ of regular plane curves, based on the principles described in Sections 3–6, is summarized below.

Minkowski sum algorithm.

1. *Construct graph $\mathcal{G}$ describing topological structure of envelope curve Γ.* Using the curve description algorithm, construct a planar graph $\mathcal{G}$ that is isotopic to the exact envelope curve Γ for $\boldsymbol{\alpha}(u) \oplus \boldsymbol{\beta}(v)$. Each edge of $\mathcal{G}$ is identified with a montone arc of Γ, generated by known arcs $u \in [a, b]$ and $v \in [c, d]$ of $\boldsymbol{\alpha}(u)$ and $\boldsymbol{\beta}(v)$, with points in one-to-one correspondence specified by the Gauss maps. This information permits approximation of the arcs of Γ, corresponding to each edge of $\mathcal{G}$, to any desired accuracy. The vertices of $\mathcal{G}$ include characteristic points of Γ, and other points of Γ on vertical lines through the characteristic points.

2. *Compute degrees in vertical strips between characteristic points of Γ.* The edges of $\mathcal{G}$ subdivide each vertical strip, between the characteristic points of Γ, into regions over which the covering degree is constant. The lowest region lies outside the Minkowski sum, and is thus of degree 0. Working upward through each region within a vertical strip, the change of degree on crossing the segment of Γ represented by each edge of $\mathcal{G}$ is obtained by evaluating (14) at a representative point of that segment.

3. *Identify edges of $\mathcal{G}$ that separate regions of zero and non-zero degree.* By culling the edges of $\mathcal{G}$ that separate neighboring regions of positive degree, we obtain a sub-graph $\mathcal{G}_b$ whose edges correspond to the true boundary segments of the Minkowski sum. If information on the degree of the covering within the Minkowski sum is desired, instead of just the boundary, the culled edges can be organized in a separate sub-graph $\mathcal{G}_i$, such that $\mathcal{G} = \mathcal{G}_b \cup \mathcal{G}_i$. In the latter case, the degree of each face delineated by the edges of $\mathcal{G}$ is also encoded in the graph representation.

4. *Approximate boundary segments to prescribed geometrical tolerance.* The edges of the graph $\mathcal{G}_b$ identify monotone segments of the Minkowski sum boundary, generated by known arcs $u \in [a, b]$ and $v \in [c, d]$ of $\boldsymbol{\alpha}(u)$ and $\boldsymbol{\beta}(v)$, with points in one-to-one correspondence specified by the Gauss maps. This allows us to approximate the boundary segments to any given geometrical accuracy. If desired, the "interior" segments of the envelope Γ can also be approximated in the same manner.

8. Other geometrical convolutions

The Minkowski sum algorithm, as described above, can be extended to other geometrical convolutions in $\mathbb{R}^2$ for which the boundary of the convolution set can be interpreted as the envelope of a differentiable one-parameter family of smooth plane curves (see Section 2.1). The basic paradigm remains unchanged—we construct a piecewise-linear graph isotopic to the envelope curve, formulate an expression that defines the change in covering degree on crossing the edges of this graph, and use these changes to identify the true boundary segments, which may then be approximated to a specified geometrical accuracy.

For other convolutions, the required adaptations to the algorithm arise in the following contexts. First, a new Jacobian condition—appropriate to the convolution under consideration—must be formulated. Second, the systems of equations that define the characteristic points of the envelope curve must be amended in accordance with the new Jacobian. Finally, a new analysis must be performed in the context of the specific convolution, to express the change in covering degree on crossing an envelope segment in terms of local properties at a representative point of that segment.

As an example of such generalizations, we consider the *Minkowski product* [37,38] of sets $\mathcal{A}, \mathcal{B} \in \mathbb{R}^2$ defined by (6), where we identify points $\mathbf{a}, \mathbf{b} \in \mathbb{R}^2$ with complex numbers $a + \mathrm{i}\alpha$, $b + \mathrm{i}\beta$ and $\times$ denotes complex multiplication. A Minkowski product of two curves may, in principle, be computed using the Minkowski sum algorithm, by invoking the map $\mathbf{z} \to \log \mathbf{z}$ and writing

$$\log(\boldsymbol{\alpha}(u) \otimes \boldsymbol{\beta}(v)) = (\log \boldsymbol{\alpha}(u)) \oplus (\log \boldsymbol{\beta}(v)).$$

Once the right-hand sum is computed, the exponential map $\mathbf{z} \to \exp(\mathbf{z})$ can be invoked to obtain the Minkowski product $\boldsymbol{\alpha}(u) \otimes \boldsymbol{\beta}(v)$. However, this approach incurs practical difficulties stemming from the multi-valued nature of the complex logarithm, the amplification of approximation errors under the exponential map, and the transcendental nature of $\log \boldsymbol{\alpha}(u)$, $\log \boldsymbol{\beta}(v)$.

A more direct algorithm is based on the *logarithmic Gauss maps* of the curves $\boldsymbol{\alpha}(u)$, $\boldsymbol{\beta}(v)$. These are simply the ordinary Gauss maps of their images $\log \boldsymbol{\alpha}(u)$, $\log \boldsymbol{\beta}(v)$ under $\mathbf{z} \to \log \mathbf{z}$. The Jacobian condition $\boldsymbol{\alpha}'(u) \parallel \boldsymbol{\beta}'(v)$ for Minkowski sums thus becomes

$$\frac{\boldsymbol{\alpha}'(u)}{\boldsymbol{\alpha}(u)} \Bigg\| \frac{\boldsymbol{\beta}'(u)}{\boldsymbol{\beta}(u)}$$

for Minkowski products, and this condition is used to identify characteristic points on the envelope curve for the Minkowski product, when constructing the piecewise-linear graph that is isotopic to the envelope. Correspondingly, one defines the *logarithmic curvatures* of $\boldsymbol{\alpha}(u)$, $\boldsymbol{\beta}(v)$ as being the "ordinary" curvatures of the curves $\log \boldsymbol{\alpha}(u)$, $\log \boldsymbol{\beta}(v)$. Whereas the ordinary curvature may be defined as the derivative

$$\kappa = \frac{\mathrm{d}\psi}{\mathrm{d}s}$$

of the tangent angle ψ with respect to arc length s, the logarithmic curvature is the derivative

$$\kappa_{\log} = r\,\frac{\mathrm{d}}{\mathrm{d}s}(\psi - \theta)$$

of the *difference* between the tangent angle ψ and polar angle θ, multiplied by the modulus r. Note that κ is invariant under translation, but not uniform scaling, of a curve—conversely, $\kappa_{\log}$ is invariant under uniform scaling, but not translation. Once the graph representing the envelope of the Minkowski product is constructed, the change in covering degree on crossing its edges can be determined from formula (14) in Lemma 5, by replacing the "ordinary" curvature vectors $\mathbf{k}$ with their logarithmic counterparts, $\mathbf{k}_{\log}$.

Although this is only a "sketch" of how the algorithm can be generalized from the computation of Minkowski sums to Minkowski products, it should be clear that the basic topological principles remain unchanged, and all the required modifications are in context-specific geometrical details. This holds for other geometrical convolutions in $\mathbb{R}^2$ that interest us.

9. Closure

A novel approach to computing Minkowski sums in $\mathbb{R}^2$ has been presented, in which topological considerations play a central role. First, a planar graph isotopic to the Minkowski sum "envelope" curve (the set of points satisfying a necessary Jacobian condition for lying on the Minkowski sum boundary) is constructed. Each face delineated by this graph is assigned a covering degree, using a simple curvature-based formula that determines the change of degree upon crossing the graph edges. The true boundary corresponds to the set of edges that separate faces of zero and non-zero degree. Once the "internal" edges are discarded, the edges that identify true boundary segments can be approximated to any desired geometrical accuracy.

By minimizing detailed geometrical computations on envelope segments that are ultimately discarded, the algorithm provides efficiency improvements over traditional methods that employ explicit geometrical approximations of the entire envelope. Moreover, the algorithm furnishes not only the nominal boundary of the Minkowski sum, but also a characterization of the variation of the covering degree over its interior—which can be useful in, for example, path planning for manufacturing and inspection applications. For brevity, the focus in this paper has been on the Minkowski sum of smooth closed curves. The method can be extended to accommodate piecewise-smooth curves and non-closed curves by appropriate treatment of the Jacobian condition at the tangent discontinuities and end points of such curves.

The Minkowski sum algorithm has been presented in the broader context of *geometrical convolutions* in $\mathbb{R}^2$. Many of the key ideas and methods of this algorithm carry over directly to other convolutions in $\mathbb{R}^2$, such as Minkowski products of complex sets, swept volumes, and shape recovery from the MAT. The necessary modifications for these contexts are concerned with formulating the appropriate Jacobian condition and the expression for the change in covering degree. Because of the inherently more complicated topological structures that can arise in three dimensions, however, a detailed study is needed to extend the algorithm to $\mathbb{R}^3$. We hope to address some of these extensions in due course.

Acknowledgements

This work was supported in part by the National Science Foundation under grants CCR-0202179 and DMS-0138411.

References

[1] K. Abdel-Malek, H.J. Yeh, Geometric representation of the swept volume using Jacobian rank deficiency conditions, Comput. Aided Design 29 (1997) 457–468.

[2] P.K. Agarwal, E. Flato, D. Halperin, Polygon decomposition for efficient construction of Minkowski sums, Comput. Geometry—Theory Appl. 21 (2002) 39–61.
[3] J.W. Ahn, M.S. Kim, S.B. Lim, Approximate general sweep boundary of 2D object, CVGIP: Graph. Models and Image Process. 55 (1993) 98–128.
[4] S. Arnborg, H. Feng, Algebraic decomposition of regular curves, J. Symbol. Comput. 5 (1988) 131–140.
[5] D.S. Arnon, Topologically reliable display of algebraic curves, ACM Comput. Graphics 17 (1983) 219–227.
[6] D.S. Arnon, G.E. Collins, S. McCallum, Cylindrical algebraic decomposition I: The basic algorithm, SIAM J. Comput. 13 (1984) 865–877.
[7] D.S. Arnon, G.E. Collins, S. McCallum, Cylindrical algebraic decomposition II: An adjacency algorithm for the plane, SIAM J. Comput. 13 (1984) 878–889.
[8] D.S. Arnon, S. McCallum, A polynomial-time algorithm for the topological type of a real algebraic curve, J. Symbol. Comput. 5 (1988) 213–236.
[9] B. Baek, S.Y. Shin, K.Y. Chwa, On computing translational swept volumes, Internat. J. Comput. Geometry Appl. 9 (1999) 293–317.
[10] D. Blackmore, M.C. Leu, F. Shih, Analysis and modeling of deformed swept volumes, Comput. Aided Design 26 (1994) 315–326.
[11] D. Blackmore, M.C. Leu, L.P. Wang, The sweep-envelope differential equation algorithm and its applications to NC machining verification, Comput. Aided Design 29 (1997) 629–637.
[12] D. Blackmore, M.C. Leu, L.P. Wang, H. Jiang, Swept volumes: a retrospective and prospective view, Neural Parallel Sci. Comput. 5 (1997) 81–102.
[13] H. Blum, R.N. Nagel, Shape description using weighted symmetric axis features, Pattern Recogn. 10 (1978) 167–180.
[14] V.G. Boltyanskii, Envelopes, Macmillan, New York, 1964.
[15] F.L. Bookstein, The line-skeleton, Comput. Graphics Image Process. 11 (1979) 123–137.
[16] R.N. Bracewell, The Fourier Transform and its Applications, third ed., McGraw-Hill, New York, 1999.
[17] J.W. Bruce, P.J. Giblin, What is an envelope?, Math. Gazette 65 (1981) 186–192.
[18] J.W. Bruce, P.J. Giblin, Curves and Singularities, Cambridge University Press, Cambridge, 1984.
[19] S. Cameron, Collision detection by four-dimensional intersection testing, IEEE Trans. Robot. Automat. 6 (1990) 291–302.
[20] P. Cellini, P. Gianni, C. Traverso, Algorithms for the shape of semialgebraic sets: a new approach, Lecture Notes in Computer Science, vol. 539, Springer, Berlin, 1991, pp. 1–18.
[21] M.P. do Carmo, Differential Geometry of Curves and Surfaces, Prentice-Hall, Englewood Cliffs, NJ, 1976.
[22] R.C. Dorf, R.H. Bishop, Modern Control Systems, 10th ed., Prentice-Hall, Upper Saddle River, NJ, 2005.
[23] G. Elber, I.-K. Lee, M.-S. Kim, Comparing offset curve approximation methods, IEEE Comput. Graphics Appl. 17 (3) (1997) 62–71.
[24] M.A. Erdmann, Protein similarity from knot theory and geometric convolutions, in: Proceedings of the Annual Conference on Research in Computational Molecular Biology, San Diego, 2004, pp. 195–204.
[25] R.T. Farouki, The approximation of non-degenerate offset surfaces, Comput. Aided Geom. Design 3 (1986) 15–43.
[26] R.T. Farouki, Pythagorean–hodograph curves, in: G. Farin, J. Hoschek, M.-S. Kim (Eds.), Handbook of Computer Aided Geometric Design, Elsevier, Amsterdam, 2002, pp. 405–427.
[27] R.T. Farouki, Minkowski combinations of complex sets—geometry algorithms, and applications, in: T. Lyche, M.-L. Mazure, L.L. Schumaker (Eds.), Curve and Surface Design: Saint-Malo 2002, Nashboro Press, 2003, pp. 123–146.
[28] R.T. Farouki, J.-C.A. Chastang, Curves and surfaces in geometrical optics, in: T. Lyche, L.L. Schumaker (Eds.), Mathematical Methods in Computer Aided Geometric Design II, Academic Press, New York, 1992, pp. 239–260.
[29] R.T. Farouki, J.-C.A. Chastang, Exact equations of "simple" wavefronts, Optik 91 (1992) 109–121.
[30] R.T. Farouki, W. Gu, H.P. Moon, Minkowski roots of complex sets, in: Geometric Modeling and Processing 2000, IEEE Computer Society Press, 2000, pp. 287–300.
[31] R.T. Farouki, C.Y. Han, Computation of Minkowski values of polynomials over complex sets, Numer. Algorithms 36 (2004) 13–29.
[32] R.T. Farouki, C.Y. Han, Solution of elementary in the Minkowski geometric algebra of complex sets, Adv. Comput. Math. 22 (2005) 325–352.
[33] R.T. Farouki, C.Y. Han, Root neighborhoods, generalized lemniscates, and robust stability of dynamic systems, Appl. Algebra Eng. Comm. Comput., 2006, to appear.
[34] R.T. Farouki, C.Y. Han, J. Hass, Boundary evaluation algorithms for Minkowski combinations of complex sets using topological analysis of implicit curves, Numer. Algorithms 40 (2005) 251–283.
[35] R.T. Farouki, J.K. Hinds, A hierarchy of geometric forms, IEEE Comput. Graphics Appl. 5 (5) (1985) 51–78.
[36] R.T. Farouki, H.P. Moon, Minkowski geometric algebra and the stability of characteristic polynomials, in: H.-C. Hege, K. Polthier (Eds.), Visualization and Mathematics III, Springer, Berlin, 2003, pp. 163–188.
[37] R.T. Farouki, H.P. Moon, B. Ravani, Algorithms for Minkowski products and implicitly-defined complex sets, Adv. Comput. Math. 13 (2000) 199–229.
[38] R.T. Farouki, H.P. Moon, B. Ravani, Minkowski geometric algebra of complex sets, Geom. Dedicata 85 (2001) 283–315.
[39] R.T. Farouki, C.A. Neff, Analytic properties of plane offset curves & Algebraic properties of plane offset curves, Comput. Aided Geom. Design 7 (1990) 83–99, 101–127.
[40] R.T. Farouki, H. Pottmann, Exact Minkowski products of N complex disks, Reliab. Comput. 8 (2002) 43–66.
[41] R.H. Fowler, The Elementary Differential Geometry of Plane Curves, Cambridge University Press, Cambridge, 1929.
[42] M. Ganter, J. Uiker, Dynamic collision detection using swept solids, ASME J. Mech. Transmissions, Automat. Design 108 (1986) 549–555.
[43] P.K. Ghosh, A mathematical model for shape description using Minkowski operators, Comput. Vision Graphics Image Process. 44 (1988) 239–269.
[44] L. Gonzalez-Vega, I. Necula, Efficient topology determination of implicitly defined algebraic plane curves, Comput. Aided Geom. Design 19 (2002) 719–743.

[45] T.A. Grandine, F.W. Klein, A new approach to the surface intersection problem, Comput. Aided Geom. Design 14 (1997) 111–134.
[46] H. Hadwiger, Vorlesungen über Inhalt, Oberfläche, und Isoperimetrie, Springer, Berlin, 1957.
[47] E.E. Hartquist, J.P. Menon, K. Suresh, H.B. Voelcker, J. Zagajac, A computing strategy for applications involving offsets, sweeps, and Minkowski operators, Comput. Aided Design 31 (1999) 175–183.
[48] J. Hass, R.T. Farouki, C.Y. Han, X. Song, T.W. Sederberg, Guaranteed consistency of surface intersections and trimmed surfaces using a coupled topology resolution and domain decomposition scheme, Adv. Comput. Math., 2006, to appear.
[49] A. Hernandez Barrera, Computing the Minkowski sum of monotone polygons, IEICE Trans. Inform. Syst. E80D (1997) 218–222.
[50] H. Hong, An efficient method for analyzing the topology of plane real algebraic curves, Math. Comput. Simulation 42 (1996) 571–582.
[51] H.K. Hwang, A Poisson geometric convolution law for the number of components in unlabelled combinatorial structures, Combin. Probab. Comput. 7 (1998) 89–110.
[52] B.M. Imani, M.A. Elbestawi, Geometric simulation of ball-end milling operations, ASME J. Manufact. Sci. Eng. 123 (2001) 177–184.
[53] K.P. Karunakaran, P.V. Shanmuganathan, N. Gupta, M. Isaac, Swept volume of a generic cutter, J. Eng. Manuf. 214 (2000) 915–938.
[54] A. Kaul, Computing Minkowski sums, Ph.D. Thesis, Columbia University, 1993.
[55] A. Kaul, R.T. Farouki, Computing Minkowski sums of plane curves, Internat. J. Comput. Geometry Appl. 5 (1995) 413–432.
[56] A. Kaul, J.R. Rossignac, Solid interpolating deformations: construction and animation of PIPS, Comput. Graphics 16 (1992) 107–115.
[57] J. Kieffer, F.L. Litvin, Swept volume determination and interference detection for moving 3D solids, ASME J. Mech. Design 113 (1991) 456–463.
[58] M.S. Kim, J.W. Ahn, S.B. Lim, An algebraic algorithm to compute the exact general sweep boundary of a 2D curved object, Inform. Process. Lett. 47 (1993) 221–229.
[59] Y.J. Kim, G. Varadhan, M.C. Lin, D. Manocha, Fast swept volume approximation of complex polyhedral models, Comput. Aided Design 36 (2004) 1013–1027.
[60] I.K. Lee, M.S. Kim, Polynomial/rational approximation of Minkowski sum boundary curves, Graph. Models Image Process. 60 (1998) 136–165.
[61] I.K. Lee, M.S. Kim, G. Elber, New approximation methods of planar offset and convolution curves, in: W. Strasser, R. Klein, R. Rau (Eds.), Geometric Modeling: Theory and Practice, Springer, Berlin, 1997, pp. 83–101.
[62] M.C. Leu, S.H. Park, K.K. Wang, Geometric representation of translational swept volumes and its applications, ASME J. Eng. Industry 108 (1986) 113–119.
[63] Z.K. Ling, T. Chase, Generating the swept area of a body undergoing planar motion, ASME J. Mech. Design 118 (1996) 221–223.
[64] Z.K. Ling, Z.J. Hu, Use of swept volumes in the design of interference free spatial mechanisms, Mechanism Mach. Theory 32 (1997) 459–476.
[65] T. Lozano-Pérez, M.A. Wesley, An algorithm for planning collision-free paths among polyhedral obstacles, Comm. ACM 22 (1979) 560–570.
[66] B.Y. Maiteh, D. Blackmore, K. Abdel-Malek, M.C. Leu, Swept-volume computation for machining simulation and virtual reality application, J. Mat. Process. Manuf. Sci. 7 (1999) 380–390.
[67] R.R. Martin, P.C. Stephenson, Sweeping of three dimensional objects, Comput. Aided Design 22 (1990) 223–234.
[68] A.E. Middleditch, Applications of a vector sum operator, Comput. Aided Design 20 (1988) 183–188.
[69] J. Milnor, Morse Theory, Princeton University Press, Princeton, NJ, 1963.
[70] H. Minkowski, Volumen und Oberfläche, Math. Ann. 57 (1903) 447–495.
[71] R.E. Moore, Interval Analysis, Prentice-Hall, Englewood Cliffs, NJ, 1966.
[72] L. Parida, S.P. Mudur, Computational methods for evaluating swept object boundaries, Visual Comput. 10 (1994) 266–276.
[73] M.S. Petković, L.D. Petković, Complex Interval Arithmetic and its Applications, Wiley-VCH, Berlin, 1998.
[74] R. Ramamurthy, R.T. Farouki, Voronoi diagram and medial axis algorithm for planar domains with curved boundaries I. Theoretical foundations & II. Detailed algorithm description, J. Comput. Appl. Math. 102 (1999) 119–141, 253–277.
[75] J.R. Rossignac, A.A.G. Requicha, Offsetting operations in solid modelling, Comput. Aided Geom. Design 3 (1986) 129–148.
[76] M.-F. Roy, A. Szpirglas, Complexity of the computation of cylindrical decomposition and topology of real algebraic curves using Thom's Lemma, Lecture Notes in Mathematics, vol. 1420, Springer, Berlin, 1990, pp. 223–236.
[77] T. Sakkalis, The topological configuration of a real algebraic curve, Bull. Austral. Math. Soc. 43 (1991) 37–50.
[78] K. Sambandan, K. Kedem, K.K. Wang, Generalized planar sweeping of polygons, J. Manuf. Syst. 11 (1992) 246–257.
[79] J. Serra, Image Analysis and Mathematical Morphology, Academic Press, London, 1982.
[80] J. Serra, Introduction to mathematical morphology, Comput. Vision Graphics Image Process. 35 (1986) 283–305.
[81] X. Song, T.W. Sederberg, J. Zheng, R.T. Farouki, J. Hass, Linear perturbation methods for topologically consistent representations of free-form surface intersections, Comput. Aided Geom. Design 21 (2004) 303–319.
[82] J.V. Uspensky, Theory of Equations, McGraw-Hill, New York, 1948.
[83] G.P. Wang, J.G. Sun, X.J. Hua, The sweep-envelope differential equation for general deformed swept volumes, Comput. Aided Geom. Design 17 (2000) 399–418.
[84] W.P. Wang, K.K. Wang, Geometric modeling for swept volume of moving solids, IEEE Comput. Graphics Appl. 6 (12) (1986) 8–17.
[85] K. Weinert, S.J. Du, P. Damm, M. Stautner, Swept volume generation for the simulation of machining processes, Internat. J. Mach. Tools Manuf. 44 (2004) 617–628.
[86] J.D. Weld, M.C. Leu, Geometric representation of swept volumes with application to polyhedral objects, Internat. J. Robot. Res. 9 (1990) 105–117.
[87] J.Z. Yang, K. Abdel-Malek, Approximate swept volume of NURBS surfaces or solids, Comput. Aided Geom. Design 22 (2005) 1–26.